Food Chemistry: Molecular Sciences 12 (2026) 100407

Contents lists available at ScienceDirect

Food Chemistry: Molecular Sciences

journal homepage: www.sciencedirect.com/journal/food-chemistry-molecular-sciences

Building *Hovenia dulcis* pseudofruit quality from proteomic and metabolomic perspectives

Gilson Gustavo Lucinda Machado [a,*], Elda Eller [b], Carlos Henrique Milagres Ribeiro [c], Carlos Alexandre Rocha da Costa [a], Sidney Vasconcelos do Nascimento [d], Sayure Mariana Raad Nahon [d], Alice de Paula de Sousa Cavalcante [d], Isa Rebecca Chagas da Costa [d], Rafael Borges da Silva Valadares [d], Elisângela Elena Nunes Carvalho [a], Eduardo Valério de Barros Vilas Boas [a,*]

[a] *Food Science Department – DCA, Federal University of Lavras – UFLA, Lavras, MG, CEP, 37200-900, Brazil*
[b] *University of Algarve, Gambelas Campus, 8005-139 Faro, Portugal.*
[c] *Department of Agriculture, Federal University of Lavras, Lavras, MG 37200-000, Brazil.*
[d] *Instituto Tecnológico Vale, Rua Boaventura da Silva 955, Belém, PA, CEP, 66050-090, Brazil*

ARTICLE INFO

Keywords:
Ripening. Proteomics. Energy metabolism. Sugars. Oxidative stress

ABSTRACT

Hovenia dulcis Thunb. (Japanese grape tree) pseudofruit exhibits a period of growth of 180 days, with maturation initiated between 120 and 150 days after anthesis (DAA). Effective ripening occurs 150 DAA, characterized by intense softening, pectic solubilization and starch-sugar conversion. Multi-omic analysis identified 496 proteins, with 222 being differentially expressed. Significant highlights included energy metabolism (Malate Dehydrogenases, Glyceraldehyde-3-phosphate Dehydrogenase, Pyruvate Kinase) and photosynthetic pathways (Ribulose-1,5-bisphosphate Carboxylase/Oxygenase, Photosystems I and II), indicating that ripening demands a high energy supply. Multivariate analysis stratified the development into three phases: chemical defense (S1-S2), metabolic transition (S3-S6), and sensory ripening (S7). The Variable Importance in Projection (VIP) score and Principal Component 1 (PC1) loadings confirmed that the transition is governed by changes in volatile compounds (2-heptanol), respiratory physiology, density, and Hue angle, with a central role for malate dehydrogenase. Pearson correlations revealed a coordinated system in which central metabolism (Glyceraldehyde-3-phosphate Dehydrogenase, Triose Phosphate Isomerase) is coupled with ethylene signaling (S-adenosylmethionine Synthetase) and antioxidant defenses (Superoxide Dismutase, Catalase, and Peroxiredoxin 2). It is concluded that *H. dulcis* development is sustained by a strategic proteometabolic network that redirects the investment from protective biomolecules toward the specialization of sensory attributes, defining the final quality of the pseudofruit.

1. Introduction

Hovenia dulcis Thunb. is a deciduous perennial tree belonging to the Rhamnaceae family, widely distributed across Asia, particularly in China, Japan, and Korea (Peng et al., 2018; Thi Ngo et al., 2021; Xu et al., 2020). The species is noted for its ethnobotanical importance, having been used for centuries in Asian culinary and medicine (Morales et al., 2017). Its various parts, including fruits, pseudofruits, seeds, leaves, roots, and bark, are extensively employed in traditional Oriental medicine due to their therapeutic properties (Song et al., 2020).

The pseudofruits of this species, popularly known as the Japanese grape tree, are the most consumed parts (Peng et al., 2018; (Song et al., 2020). However, the seeds also stand out as a significant source of natural antioxidants, offering protective effects against oxidative stress-related conditions, such as alcoholic liver disease (Meng et al., 2020). Similarly to cashew apple (*Anacardium occidentale*), the floral peduncle develops into a flavorful and succulent pseudofruit. During maturation, the twisted peduncles of the Japanese grape tree become swollen, irregular, and fleshy (3–7 mm in diameter), acquiring a reddish-brown coloration and a sweet flavor due to high sucrose content

* Corresponding author.
E-mail addresses: gilsonguluma@gmail.com (G.G.L. Machado), evbvboas@ufla.br (E.V. de Barros Vilas Boas).

https://doi.org/10.1016/j.fochms.2026.100407
Received 15 January 2026; Received in revised form 12 April 2026; Accepted 20 April 2026
Available online 25 April 2026

(De Biaggi et al., 2020; Yang et al., 2019). Beyond *in natura* consumption, these pseudofruits can be processed into wines, juices, fermented alcoholic beverages, jams, jellies, and raisins, or used as a source of antioxidants in processed meat products (Machado & Gonçalves, 2021; Pinto et al., 2017; Schaefer et al., 2022; Xu et al., 2020).

Changes in physical properties and nutritional composition during maturation of *H. dulcis* pseudofruits have been reported in the literature (Maieves et al., 2015; Maieves et al., 2017). The chemical composition of these pseudofruits is characterized by high sugar levels and presence of bioactive compounds such as flavonoids, lignans, sesquiterpenoids, triterpenoids, and benzoic acid. These substances provide the pseudofruits with diverse biological properties, including antioxidant, antimicrobial, antidiabetic, anti-inflammatory, anti-obesity, and laxative activities (Maieves et al., 2015; Choi et al., 2017; Morales et al., 2017; Peng et al., 2018; Yang et al., 2019; De Biaggi et al., 2020; Oh et al., 2020; Song et al., 2020; De Godoi et al., 2021; Sferrazza et al., 2021; Thi Ngo et al., 2021). Furthermore, studies indicate that both the seeds and pseudofruits of *H. dulcis* possess phytotherapeutic potential in treating various diseases, particularly alcoholism and liver disorders (Choi et al., 2017; Kim et al., 2017; Kim et al., 2023; Qiu et al., 2019; Wang et al., 2017).

Despite the extensive knowledge regarding the pharmacological, nutritional, and functional properties of the species, the molecular processes regulating the synthesis and accumulation of nutrients and bioactive compounds throughout pseudofruit development remain unknown. Therefore, investigating these mechanisms could significantly contribute to the valorization of the species and expand its application potential in the food and pharmaceutical industries. Moreover, understanding the molecular mechanisms underlying the construction of quality in fruits and pseudofruits is fundamental to supporting genetic improvement and domestication efforts, as well as guiding best production practices, with emphasis on mineral fertilization, irrigation, and thinning.

In this context, proteomic analysis emerges as an essential tool for understanding the molecular mechanisms involved in fruit and pseudofruit development. This approach allows for the global identification and quantification of proteins expressed at different developmental stages, providing detailed information on the biochemical processes underlying maturation and the production of secondary metabolites (Chen et al., 2020). Deciphering the molecular determinants of quality is vital for subsidizing domestication and breeding programs, as well as directing precision agronomic practices, such as mineral fertilization management and harvest point optimization. Consequently, the present study proposes an integrated multi-omic investigation, combining physical, physicochemical, and chemical analyses with high-resolution proteomics. The objective is to map biological transformations from anthesis to ripening, elucidating how the coordination between central metabolism and specialized metabolite pathways defines the technological potential of this species.

2. Materials and methods

2.1. Experimental design

The experiment followed a completely randomized design (CRD), consisting of seven treatments (developmental stages, from S1 to S7) and three replicates. Three distinct trees were used as biological replicates for each treatment. All laboratory analyses were performed in technical triplicate.

2.2. Plant material

H. dulcis pseudofruits were harvested from trees located at the Federal University of Lavras (UFLA), Minas Gerais, Brazil (latitude 21° 14′ 43“ S, longitude 44° 59’ 59” W, and altitude of 919 m). The selected trees were situated in the same experimental area under uniform edaphoclimatic conditions, ensuring that all biological replicates were exposed to the same environmental factors. Harvest dates were defined based on the peak flowering period, which occurred on October 25, 2022. Sampling intervals of 30 days were established, considering the long developmental cycle of the pseudofruit, as previously described (Maieves et al., 2015). For each developmental stage, approximately 500 g of pseudofruits were collected from different quadrants of the canopy of each of the three independent trees, to ensure the representativeness of the biological material and minimize environmental variations. The complete developmental cycle of the pseudofruits spanned 210 days, resulting in seven sample collections designated as S1, S2, S3, S4, S5, S6, and S7, corresponding to 30, 60, 90, 120, 150, 180, and 210 days after anthesis (DAA), respectively (Fig. 1).

Pseudofruits were collected from November 2022 to May 2023 and transported in insulated boxes to the Fruit and Vegetable Postharvest Laboratory at the Federal University of Lavras. In the laboratory, the *H. dulcis* pseudofruits consisting of the fleshy peduncle and the seeds attached to their external surface were separated. A portion of the pseudofruits was pulverized using liquid nitrogen and stored at −80 °C (Coldlab, model CL374-86 V, Piracicaba, Brazil) for subsequent molecular and physicochemical analyses; the seeds were discarded.

Texture, respiratory activity, color, density, and mass analyses were performed on the fresh peduncles.

2.3. Analyses

2.3.1. Mass

The mass of 10 pseudofruits per replicate was evaluated using a semi-analytical balance (Mettler Toledo, model PC 2000, Greifensee, Switzerland), and the results were expressed in grams (g).

2.3.2. Respiratory rate

Approximately three grams of pseudofruits were placed in 50 mL glass flasks, hermetically sealed, and maintained at a controlled temperature of 25 °C to ensure metabolic homogeneity. The CO_2 concentration was determined using a PBI Dansensor gas analyzer (CheckPoint model, Ringster, Denmark), after 1 h 30 min of rest. Results, expressed as % of CO_2, were converted to mL CO_2 kg^{-1} h^{-1}.

2.3.3. Density

Density was measured using an analytical balance (Shimadzu, model AUX 320, Kyoto, Japan) equipped with a specific density measurement kit, model SMK 401.

2.3.4. Coloration

Thirty pseudofruits per replicate were analyzed for skin color using a colorimeter (Konica Minolta, model CR-400, Osaka, Japan) in the L*, a*, b*, h°, C* color space of the International Commission on Illumination (CIE).

2.3.5. Total chlorophyll

Total chlorophyll content was determined spectrophotometrically

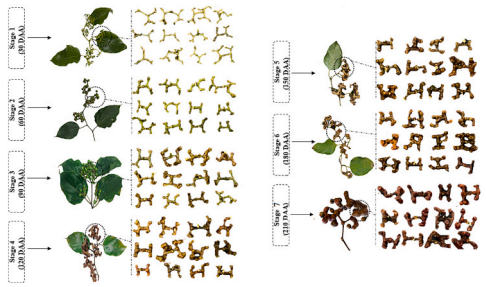

Fig. 1. *H. dulcis* pseudofruits at different stages of development.

(Biochrom, model EZ Read 2000, Cambridge, United Kingdom) in accordance to Paradiso et al. (2018), with results expressed in mg 100 g^{-1} of sample.

2.3.6. Total carotenoids

Carotenoids were extracted and quantified using the spectrophotometric method (Biochrom, model EZ Read 2000, Cambridge, United Kingdom) as described by Rodriguez-Amaya (2001), with adaptations. Results were expressed in mg 100 g^{-1} of sample.

2.3.7. Anthocyanins

Total anthocyanin content was estimated spectrophotometrically according to Lee and Francis (1972), adapted by Barcia et al. (2012). Results were expressed as milligrams of cyanidin-3-glucoside 100 g^{-1} of sample.

2.3.8. Starch

Extraction was performed according to Zanandrea et al. (2009). Glucose resulting from starch hydrolysis was determined as described by Dische (1962), using anthrone reagent (Sigma-Aldrich, St. Louis, MO, USA). Results were expressed as grams of glucose 100 g^{-1} os sample.

2.3.9. Firmness

Determined in 30 pseudofruits per replicate at three different points using a texture analyzer (Stable Micro Systems, model TA.XT2i, Godalming, United Kingdom) with a TA39 cylindrical probe (2 mm diameter). Test parameters were: pre-test speed 1 mm/s, test speed 2.0 mm/s, post-test speed 10.00 mm/s, and a trigger force of 5 g. Results were expressed in Newtons (N).

2.3.10. Soluble and Total pectin

Total and soluble pectins were extracted by precipitation in a hydroethanolic solution (95%) (Sigma-Aldrich, St. Louis, MO, USA) according to McCreaddy and McComb (1952). Quantificiation was performed via colorimetric method (Biochrom, model EZ Read 2000, Cambridge, United Kingdom) at 530 nm using carbazol (Sigma-Aldrich), as the chromogenic agent (Bitter & Muir, 1962). Results were expressed in mg of galacturonic acid 100 g^{-1} of sample.

2.3.11. pH, titratable acidity (TA), and soluble solids (SS)

Samples were ground in water at a 1:3 (*w/v*) ratio and filtered through organza. The filtrate was used for pH, TA, and SS determinations. pH was measured using a digital pH meter (TECNAL, TEC-7, Piracicaba, Brasil), calibrated with buffer solutions (pH 4.0 and 7.0). TA was determined by titration with 0.01 N sodium hydroxide (NaOH; Sigma-Aldrich, St. Louis, MO, USA) using phenolphthalein (Sigma-Aldrichas) as an indicator, according to Association of Official Analytical Chemistry (2019). Results were expressed in mg of malic acid 100 $g^{-1}$of sample. SS were determined using a digital refractometer (ATAGO, model PR-100, Tokio, Japan) with automatic temperature compensation, and the results were expressed as %, as described by Association of Official Analytical Chemistry (2019).

2.3.12. Total sugars (TS)

Total sugars were extracted in 95% ethanol and determined spectrophotometrically (Biochrom, model EZ Read 2000, Cambridge, United Kingdom) at 620 nm after alcohol evaporation, using anthrone (Sigma-Aldrich, St. Louis, MO, USA) as the chromogenic agent (Dische, 1962). The results were expressed as grams of glucose 100 g^{-1}.

2.3.13. Vitamin C

Vitamin C content was determined by a colorimetric method using 2,4-dinitrophenylhydrazine (Sigma-Aldrich, St. Louis, MO, USA), and the results were expressed as mg of ascorbic acid 100 g^{-1} (Stroheker and Henning, 1967).

2.3.14. Scanning Electron microscopy (SEM)

For the cell wall morphological analysis, samples of pseudofruits at different developmental stages were cut with a scalpel and placed into microtubes containing modified Karnovsky fixative, where they were kept until sample preparation. For specimen preparation, the samples were fractured in liquid nitrogen and dehydrated through an acetone gradient, followed by critical-point drying (Bal-Tec, model CPD 030, Balzers, Liechtenstein). Subsequently, the specimens were mounted on stubs, coated with gold using a sputter coater (Bal-Tec, model CPD 030, Balzers, Liechtenstein), and observed under a field-emission scanning electron microscope (Tescan, model MIRA3, Brno, Czech Repuclic) at an accelerating voltage of 10 keV.

2.3.15. Histochemistry

2.3.15.1. Dehydration. Samples fixed in Karnovsky solution were dehydrated through a graded ethanol series (25%, 50%, 75%, 90%, and two changes of 100%), with vacuum applied during the first four steps. In the final steps, the tubes were left open. After dehydration, infiltration was carried out with a mixture of activated resin and ethanol (1:1, *v*/v), followed by vacuum for 15 min, and the samples were stored at 4 °C for 48 h. Subsequently, samples were immersed in pure resin, subjected to vacuum, and stored for 94 h.

2.3.15.2. Embedding. For embedding, the inclusion resin was prepared by mixing activated resin and hardener (7.5:0.5 mL) on ice. The molds were partially filled and placed in an oven at 60 °C for 10 min. The samples were added before the second polymerization step, which lasted 24 h. After curing, the blocks were mounted on wooden cubes and stored with silica gel for 24 h. Sections were obtained using an ultramicrotome (Reichrt-jung, Ultracut model, Vienna, Austria). The sections were then mounted on slides, stained with Lugol's solution, and observed under a stereoscopic microscope with epifluorescence (Nikon, model SMZ 1500, Tokyo, Japan).

2.3.16. Phenolic profile

Phenolic compounds were analyzed as described by Machado et al. (2024b), using high-performance liquid chromatography (HPLC-DAD-UV–Vis). Identification was performed based on retention times, which were compared with standards of catechin (CAT), vanillin (VAN), resveratrol (RES), gallic (GA), chlorogenic (CGA), caffeic (CA), syringic (SA), *p*- coumaric (*p*-CA), *o*- coumaric (*o*-CuA), *m*-coumaric (*m*-CuA), ferulic (FA), rosmarinic (RA), and *trans*-cinnamic (*t*-CA) acids in methanol. The results were expressed in mg per 100 g^{-1} of fresh sample.

2.3.17. Volatile compounds

Volatile compounds of *H. dulcis* were analyzed using headspace solid-phase microextraction coupled with gas chromatography–mass spectrometry (HS-SPME-GC–MS), according to Da Costa et al. (2024). Samples (5 g) were placed in 20 mL vials and equilibrated at 40 °C for 30 min, followed by extraction using a DVB/CAR/PDMS fiber (50/30 μm). The determination was performed on a GC–MS system (Shimadzu) equipped with an SLB-5MS column (30 m × 0.25 mm × 0.25 μm), using helium (1.0 mL min^{-1}) as the carrier gas. The temperature ramp started at 40 °C (held for 30 min), with an increase of 3 °C min^{-1} up to 220 °C. The interface and ion source temperatures were set at 240 °C and 220 °C, respectively. Identification was conducted by comparing mass spectra with the Wiley 8 and NIST libraries.

2.3.18. Proteomics

2.3.18.1. Freeze-drying. The samples were frozen at −75 °C (Coldlab, model CL 120–86 V, Piracicaba, Brazil) for 24 h and then freeze-dried (Edwards, model L4KR, São Bernardo do Campo, Brazil) at −30 °C under a vacuum pressure of 0.998 mbar for 72 h in the dark (Meira et al.,

2023). Once freeze-dried, the samples were transported to the Vale Technological Institute, located in the city of Belém (1° 27′ 18″ S, 48° 30′ 9″ W), the capital of the state of Pará, northern Brazil, where they underwent proteomic analyses.

2.3.18.2. Protein extraction and quantification. Proteomic analysis was performed according to the protocol described by Do Nascimento et al. (2022). The fruits were ground in liquid nitrogen until they reached a fine powder consistency. To each sample, 10 mL of extraction buffer containing sucrose (1.5 M), Tris-HCl (1.5 M, pH 8), 10% sodium dodecyl sulfate (SDS), 100 mM phenylmethylsulfonyl fluoride (PMSF), polyvinylpolypyrrolidone (PVPP), and ultrapure water were added, along with 100 µL of protease inhibitor cocktail (P8340 Sigma-Aldrich) and 500 µL of β-mercaptoethanol. After five 30-s sonication cycles (Bandelin Electronic, Berlin, Germany), the extracts were divided into ten microtubes, each with the addition of 700 µL of phenol per tube. The samples were vortexed (MixMate, Eppendorf AG, Hamburg, Germany) and centrifuged (5810 R, Eppendorf, Hamburg, Germany) twice at 20,800 x g for 8 min to separate the phenolic phase and remove any aqueous phase or SDS residues. Then, 1300 µL of ammonium acetate in methanol was added for protein precipitation for approximately 24 h at −80 °C (Innova U570, Eppendorf, Hamburg, Germany). Another centrifugation was performed at 20,800 x*g* for 8 min, and the supernatant was discarded. The precipitate was transferred to a new microtube and washed four times with 80% acetone. A final wash with 70% ethanol was performed, and the precipitate was air-dried in a vacuum concentrator (miVac DNA, Genevac Ltd., Ipswich, UK) for approximately 7 min. The extracts were solubilized in 200 µL of 0.2% RapiGest (Waters, Milford, MA, USA) and stored for further analysis.

2.3.18.3. Protein digestion. The digestion preparation was initially performed by reducing proteins with dithiothreitol (DTT, 5 mM, Sigma –Aldrich, St. Loius, MO, USA), incubating for 25 min at 56 °C, followed by alkylation with iodoacetamide (IAA, 14 mM; Sigma-Aldrich) for 30 min. Residual IAA was removed by adding DTT (5 mM) again, with a 15-min incubation. Samples were diluted at a 1:5 ratio with ammonium bicarbonate (50 mM), followed by the addition of $CaCl_2$ (1 mM). The enzymatic digestion was carried out sequencing-grade modified trypsin (20 ng/µL; Promega, Madison, WI, USA) for 16 h at 37 °C. Subsequently, trifluoroacetic acid (TFA; Sigma-Aldrich) was added at a final concentration of 0.4% of the sample volume to stop the enzymatic reaction.

2.3.18.4. Protein identification and data analysis. Five micrograms of peptides were analyzed using a NanoACQUITY UPLC ultraperformance liquid chromatography system (Waters, Milford, MA, USA), configured for two-dimensional fractionation. The proteomic profile was determinad through a label-free quantification (LFQ) approach using data-independent acquisition (MS^E). For the first dimension, a 5 µm XBridge™ BEH130 C18 analytical column (300 µm × 50 mm) was used at a flow rate of 2 µL min^{-1}. The second dimension comprised a trap C18 column, 5 µm (180 µm × 20 mm), and an analytical 1.7 µm BEH130™ C18 column (100 µm × 100 mm) at a flow rate of 400 nL min^{-1}. Samples were separated into 5 fractions using acetonitrile gradients of 10.8, 14.0, 16.7, 20.4, and 65.0%. The chromatograph was directly coupled to an ESI-Q-ToF Synapt G2S mass spectrometer (Waters) operating in positive mode with continuous fragmentation (MSE), with collision energy oscillating between 5 and 40 eV. Mass spectra were acquired within a range of 50 to 1200 Da, with a scan time of 0.5 s and an interscan interval of 0.1 s. Peak width and mass spectrum resolution were set to automatic mode. The peptide (lockmass) [Glu-1]-fibrinopeptide, with a mass of 785.4827 Da and + 2 charges state, was used as reference and read every 30 s (according to lockmass spray settings).

Proteomic data were processed using Progenesis QI v4.2 software (Waters) for identification and quantification, using the UniProt TrEMBL database restricted to the Viridiplantae taxonomy (UniProtKB/Swiss-Prot, uniprot.org). Peptide identification was accepted for probabilities above 90% and proteins above 95%. Significant differences in protein abundance were determined by one-way ANOVA ($p < 0.05$). To minimize false positives, a False Discovery Rate (FDR) correction was applied, and only proteins with a q-value <0.1 were considered significant. Functional annotation of proteins was performed using Blast2GO version 4.0 (Biobam, Valencia, Spain). PCA and the heatmap were generated with the ClustVis web tool (University of Tartu, Tartu, Estonia, https://biit.cs.ut.ee/clustvis/); using Euclidean distance for the heatmap clustering. Protein-protein interaction networks and functional enrichments were inferred based on functional analysis with STRING version 12.0 (STRING Consortium, http://string-db.org/, accessed on March 23, 2025), using *Arabidopsis thaliana* homologous proteins as the reference species.

2.3.19. Statistical analysis

Statistical analyses were conducted using the SISVAR software (Ferreira, 2010), and the selection of regression models was refined in GraphPad Prism 8.0.1. The corrected Akaike Information Criterion (AICc) was adopted to ensure parsimony and avoid anomalous fluctuations. For each variable, first, second, and in specific cases of clear biological trends third-order models were compared. Higher-order models were only maintained when the ΔAIC and the correction probability demonstrated unequivocal superiority over simpler models, thereby preventing overfitting.

Statistical analysis and integration of proteomics, metabolomics, and physicochemical data were performed using the MetaboAnalyst 6.0 platform. Data were organized into abundance matrices and subjected to pre-processing for missing value imputation through the LOD (Limit of Detection) method, replacing non-detected values with 1/5 of the lowest positive value for the variable.

To reduce technical variability and normalize data distribution, Log10 transformation was applied, followed by Auto-scaling (mean-centering divided by the standard deviation). Correlation analysis was performed using the Pearson coefficient (r) to evaluate linear associations between proteins and metabolites. Hierarchical clustering was conducted based on Euclidean distance and Ward's algorithm to identify co-regulation blocks during ripening. Additionally, multivariate analyses such as PCA and PLS-DA (including VIP score calculation) were employed to identify the primary biomarkers for the different maturation stages.

3. Results and discussion

3.1. Physical, physicochemical, and chemical changes associated with the quality formation of *H. dulcis* pseudofruits during development

The mass of the *H. dulcis* pseudofruits analyzed increased 14-fold, from 0.202 g to 3.052 g, 14-foldn 30 and 180 days after anthesis (DAA), followed by a reduction up to 210 DAA (Fig. 2a, $p < 0.05$). Therefore, the first 180 days of pseudofruit development are characterized by growth driven by cell division and expansion. The reduction observed after 180 DAA can be associated with water loss resulting from respiration and transpiration, as well as the intensification of catabolism, which is common during ripening and senescence. According to Saltveit (2019), water loss in fruits as observed in the present experiment is common during ripening and may stem from the respiratory process as well as physiological and biochemical changes that increase with transpiration.

In short, the aerobic respiratory process consists of the oxidation of glucose, derived from organic compounds present in cells, and its transformation into water, carbon dioxide, and chemical energy. A reduction of 93.76% in the respiratory rate of the analyzed pseudofruits was observed throughout the studied developmental period, following a pattern typical of non-climacteric fruits (Fig. 2b, $p < 0.05$). Climacteric fruits exhibit a peak in CO_2 production before, during, or after ripening,

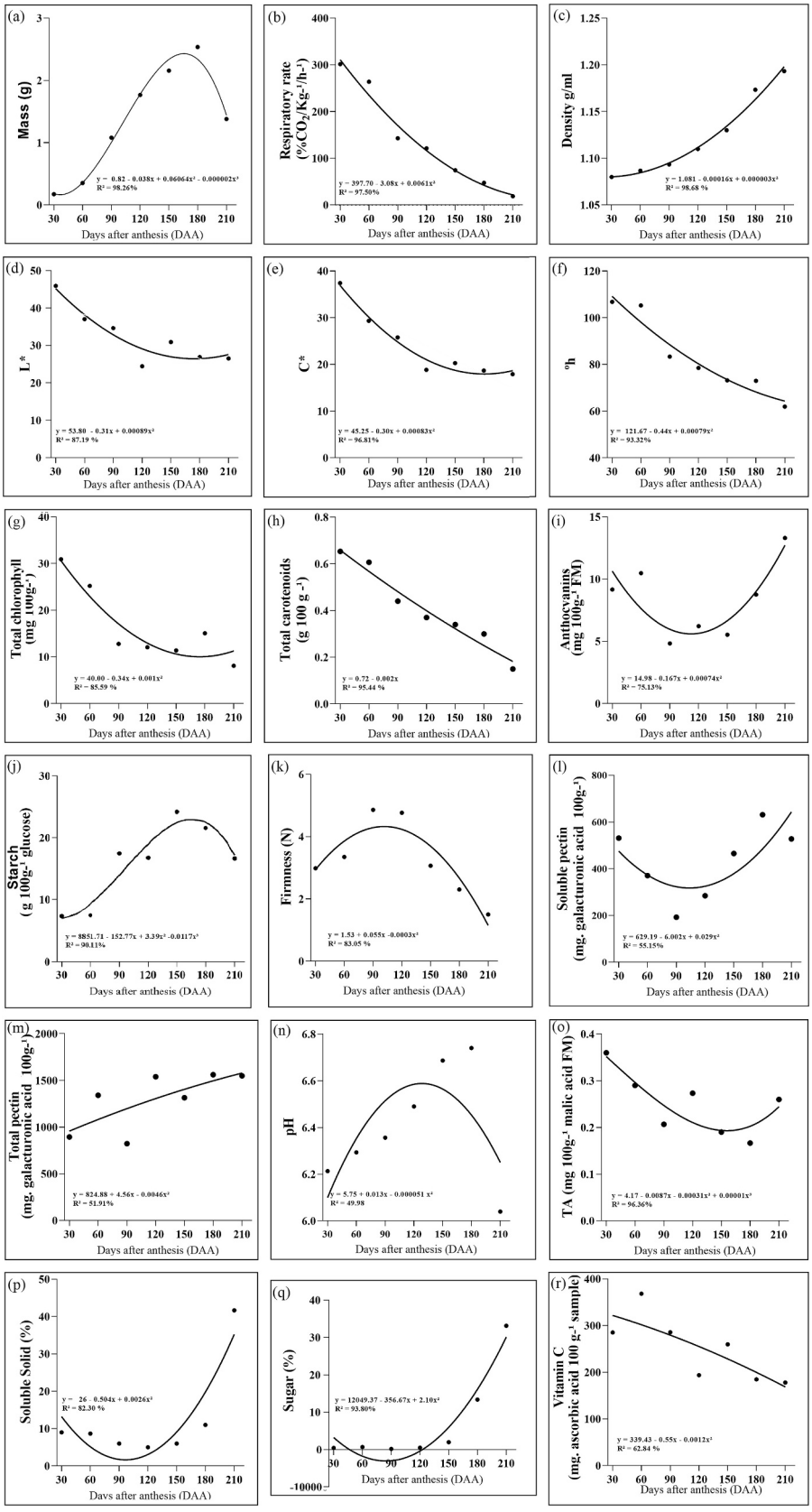

Fig. 2. Physical, physicochemical, and chemical changes during the development of *H. dulcis* pseudofruits.

which does not return to original levels even after the decline. Since transient increases in respiratory activity were not identified, especially during the ripening and senescence of the pseudofruits, it is suggested that they exhibit a typical non-climacteric behavior. While the current data suggests a non-climacteric pattern, the observed starch variations justify future high-resolution monitoring to provide a definitive physiological characterization.

The pseudofruits exhibited a quadratic behavior regarding density (from 1.06 to 1.18 g mL^{-1}) from 30 to 210 days of development (Fig. 2c, $p < 0.05$). This behavior can be explained by the translocation of photoassimilates from the leaves to the fruits and their subsequent transformation into various organic compounds responsible for the construction of quality, with little air accumulation in the intra- and extracellular spaces. Lower densities suggest a greater accumulation of gases, such as O_2 and CO_2, among other volatile compounds, particularly within the parenchymatous tissue, which reduces mass accumulation relative to the volume of the plant organs.

Despite the decarboxylation of organic matter associated with increased catabolism, water loss leads to the concentration of dry matter, which may be linked to the increase in density. The release of gases from inside the fruits, whether due to cellular decompartmentalization or the intensification of volatile emanation, both common during ripening and senescence, can contribute to the rise in density. Indeed, volatile compounds are characterized by low molecular mass, and typically, the higher their concentration, the lower the density, as they occupy the space of heavier compounds. Furthermore, water loss tends to reduce fruit volume through shriveling, which consequently leads to an increase in density, since volume and density are inversely proportional quantities.

Significant changes in the skin color of *H. dulcis* pseudofruits were confirmed throughout their development (Fig. 2 d, e, f, $p < 0.05$). A decreasing quadratic behavior was observed for the variables L*, C*, and h°, respectively. The reduction in L* highlights the darkening of the pseudofruits during development. The decrease in C* values indicates lower color vividness or saturation, suggesting that the pseudofruits lost the intense coloration present in the early stages. Meanwhile, the reduction in h° points to a shift in hue from green to yellowish-red, directly associated with the color transition characteristic of ripening. By the end of the developmental process, the pseudofruits of the Japanese grape tree exhibited a yellowish-red coloration (Fig. 1), typical of the mature pseudofruits under study (Machado et al., 2022). A reduction in L*, C*, and h° variables was also reported by Sehn et al. (2021) when evaluating the same pseudofruit at three developmental stages, indicating a consistent pattern in skin color changes across different regions.

A quadratic behavior was observed for the total chlorophyll content throughout the development of the pseudofruits of the Japanese grape tree (Fig. 2g, $p < 0.05$). Intense degradation of the pigment was noted during the first 90 DAA, followed by a stabilizing trend. Chlorophylls are pigments responsible for photosynthesis, especially in leaves, and for the greenish coloration of plants. The intense degradation of chlorophylls in the first 90 days of development coincides with the shift in h° from the yellow/green quadrant (90 to 180°) to the red/yellow quadrant (0 to 90°) (Fig. 2f). Therefore, as the concentration decreases from 30 to approximately 10 mg 100 g^{-1}, chlorophylls no longer impact the greenish skin coloration of the pseudofruits of the Japanese grape tree (Fig. 1 and Fig. 2f). It is noteworthy that chlorophyll degradation is a process manifested at various stages of fruit development, particularly during ripening (Kapoor et al., 2022).

As observed for chlorophyll, a reduction in the total carotenoids of the pseudofruits of the Japanese grape tree was noted, although it occurred in an intense and linear manner throughout the entire development (Fig. 2h, $p < 0.05$). The presence of carotenoids in young fruits indicates that the yellowish-red coloration during ripening is due to the unmasking of these pigments as a result of chlorophyll degradation, rather than their synthesis.Since carotenoids are essential components of the pigment-protein complexes in thylakoids, the regulation of carotenogenesis in green tissues appears to be linked to the formation of chlorophylls, proteins, lipids, and chloroplast development. This highly regulated process is not yet fully understood; however, it is known that light and its intensity play a crucial role in regulating carotenoid formation within the chloroplast (Bramley, 2002).

Anthocyanins, pigments that provide colors typically ranging from blue to red, were quantified in pseudofruits of the Japanese grape tree (Fig. 2i). Anthocyanin levels dropped from approximately 10 mg 100 g^{-1} at 60 DAA to about 5 mg 100 g^{-1} at 90 DAA. An increase was observed starting from 150 DAA, with approximately 12 mg 100 g^{-1} quantified at 210 DAA. In a previous study, Machado et al. (2022) were unable to identify anthocyanins in the pseudofruits of the Japanese grape tree. Failures in the extraction process, as well as in the determination method, may be the causes for the lack of anthocyanin identification in the pseudofruit. However, the influence of genetic and edafoclimatic factors on the synthesis and degradation of this pigment cannot be ruled out. The pigment analyses (Figures g, h, i) indicate that the color changes in the pseudofruit of Japanese grape tree (Fig. 1 and Figs. 2 d, e, f) are associated with shifts in chlorophylls, carotenoids, and anthocyanins.

The levels of SS and TS kept stable during first 150 days of development, while starch content increased by more than 190% (Fig. 2 j, p, q). From then on, SS and TS incresed and the starch content dropped. Sugars seem to be the principal SS of pseudofruit from 150 days of development, but not before that. In fact, the sugars are the majoritary compounds of SS in the most of fruit, although oligosaccharides, soluble pectins, and organic acids also contribute to that fraction. The observed increase in sugars and, consequently, in SS, can be related to the translocation of photoassimilates and, mainly, starch degradation (Fig. 2 j, p, q and Fig. 3 a and b). It is noteworthy that sucrose is the main translocation sugar from leaves to fruits, and its accumulation and interconversion into glucose and fructose determine the increase in TS. Furthermore, fruits that accumulate starch typically have this polysaccharide enzymatically hydrolyzed during ripening, resulting in an increase in sugars and SS (Cordenunsi-Lysenko et al., 2019).

Scanning electron microscopy (SEM) and histochemical analyses (Fig. 3 a, b) demonstrate changes in cellular structure and starch distribution during ripening, corroborating the previous statement.

The firmness of the pseudofruits exhibited a quadratic pattern, increasing during the first 90 DAA and decreasing from 120 DAA onward (Fig. 2k, $p < 0.05$). Fluctuations in total pectin content (Fig. 2m) were observed throughout development, although an increase from 894 to 1549 mg 100 g^{-1} was recorded between the first and last day of evaluation. Soluble pectin content (Fig. 2l) decreased from 531 to 192 mg 100 g^{-1} between 30 and 90 DAA, then increased to reach 631 mg 100 g^{-1} at 180 DAA and decreased again to 527 mg 100 g^{-1} at 210 DAA.

Titratable acidity (TA) and pH are inversely related variables. A decrease in TA of the Japanese raisin tree pseudofruits was observed alongside an increase in pH from 30 to 180 DAA, followed by a reversal of these trends up to 210 DAA (Fig. 2n and o). The rise in pH generally occurs due to a reduction in the concentration of hydrogen ions released by organic acids, which are consumed during the respiratory process (Barragán-Iglesias et al., 2018). Thus, the consumption of organic acids was prominent at 180 DAA. In the subsequent 30 days, the increase in TA can be associated with the concentration of organic acids resulting from transpiration losses, rather than their synthesis, as the final stage of development is typically dominated by catabolic processes.

Fruit texture is influenced by water and polysaccharides, with firmness being one of the most important aspects of this quality attribute in fruits. During growth, fruits tend to be firmer due to the synthesis of structural compounds such as starch and cell wall components (Machado et al., 2024), like the pectin observed in the Japanese grape tree pseudofruits. On the other hand, during ripening, softening tends to be conspicuous in most fruits (Machado et al., 2024), as also observed here. Therefore, the presence of starch and pectins (Fig. 2, j, l, and m) can be associated with the firmness of the Japanese grape tree

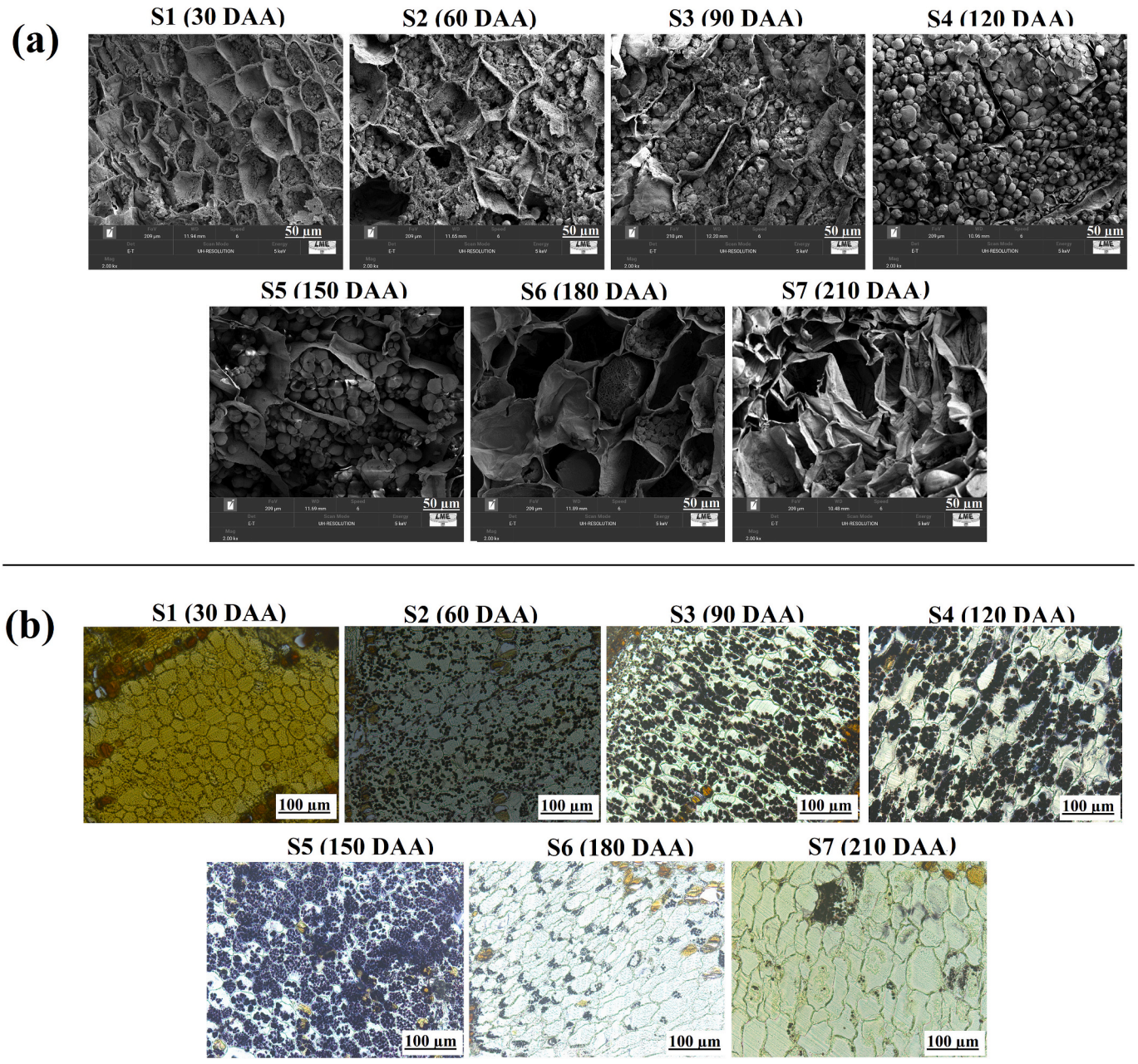

Fig. 3. (a) Scanning electron microscopy (SEM) and (b) histochemistry of the *Hovenia dulcis* pseudofruits throughout development.

pseudofruits. The drop in firmness noted from 120 DAA (Fig. 2 k) can be related to the increase in pectic solubilization (Fig. 2 l, m), resulting from its depolymerization starting at 90 DAA, and to starch hydrolysis (Fig. 2 j) starting at 180 DAA. Furthermore, depolymerization, with the consequent solubilization of pectins, results in the release of oligosaccharides, contributing to the rise in SS content (Fig. 2 p) (Beckles, 2012).

The vitamin C content of the Japanese grape tree pseudofruits increased from 285 to 368 mg 100 g^{-1} between 30 and 60 DAA, followed by a downward trend reaching approximately 184 and 178 mg 100 g^{-1} at 180 and 210 DAA, respectively (Fig. 2 r). This reduction can be attributed to the activity of enzymes such as ascorbate oxidase, peroxidases, catalases, and superoxide dismutase, which participate in ascorbic acid metabolism (Mellidou et al., 2012).The vitamin C content found in mature Japanese grape tree pseudofruits (178 mg 100 g-^{1}) is higher than that reported by Machado et al. (2022), who observed values ranging from 90.88 to 117.06 mg 100 g^{-1} for the same mature pseudofruit. This indicates that the same pseudofruit can exhibit variations in vitamin C synthesis and degradation, possibly influenced by factors such as cultivation conditions, variety, and developmental stage. It is noteworthy that approximately 50 g of the mature produce would be sufficient to meet the daily requirements of adults for this vitamin. On the other hand, pseudofruits in the early stages of development could be used as raw material for vitamin C extraction by the pharmaceutical or cosmetic industries.

Based on the physical, physicochemical, and chemical analysis results, it can be inferred that *H. dulcis* pseudofruits extended their growth over 180 DAA. The drop in firmness, stabilization of chlorophyll degradation, and the onset of pectic solubilization between 120 and 150 days suggest that maturation began during this period. On the other hand, ripening, the final stage of maturation in which fruits and pseudofruits become attractive to seed dispersal agents and suitable for consumption, started from 150 DAA, considering the intense softening accompanied by pectic solubilization, a consistent increase in sugars and soluble solids, and a rise in anthocyanins, which are primarily

responsible for the typical coloration of mature pseudofruits (Figs. 1 and 2). Furthermore, the photomicrographs and histochemical results support the finding that ripening began at 150 DAA, given the structural breakdown of amyloplasts and cell walls, as well as starch degradation phenomena typical of late development. In summary, *H. dulcis* pseudofruit development comprised 180 days of growth (stages S1-S6). Maturation overlapped this period from 120 DAA (stages S4-S7), and ripening began at 150 DAA (stages S5-S7).

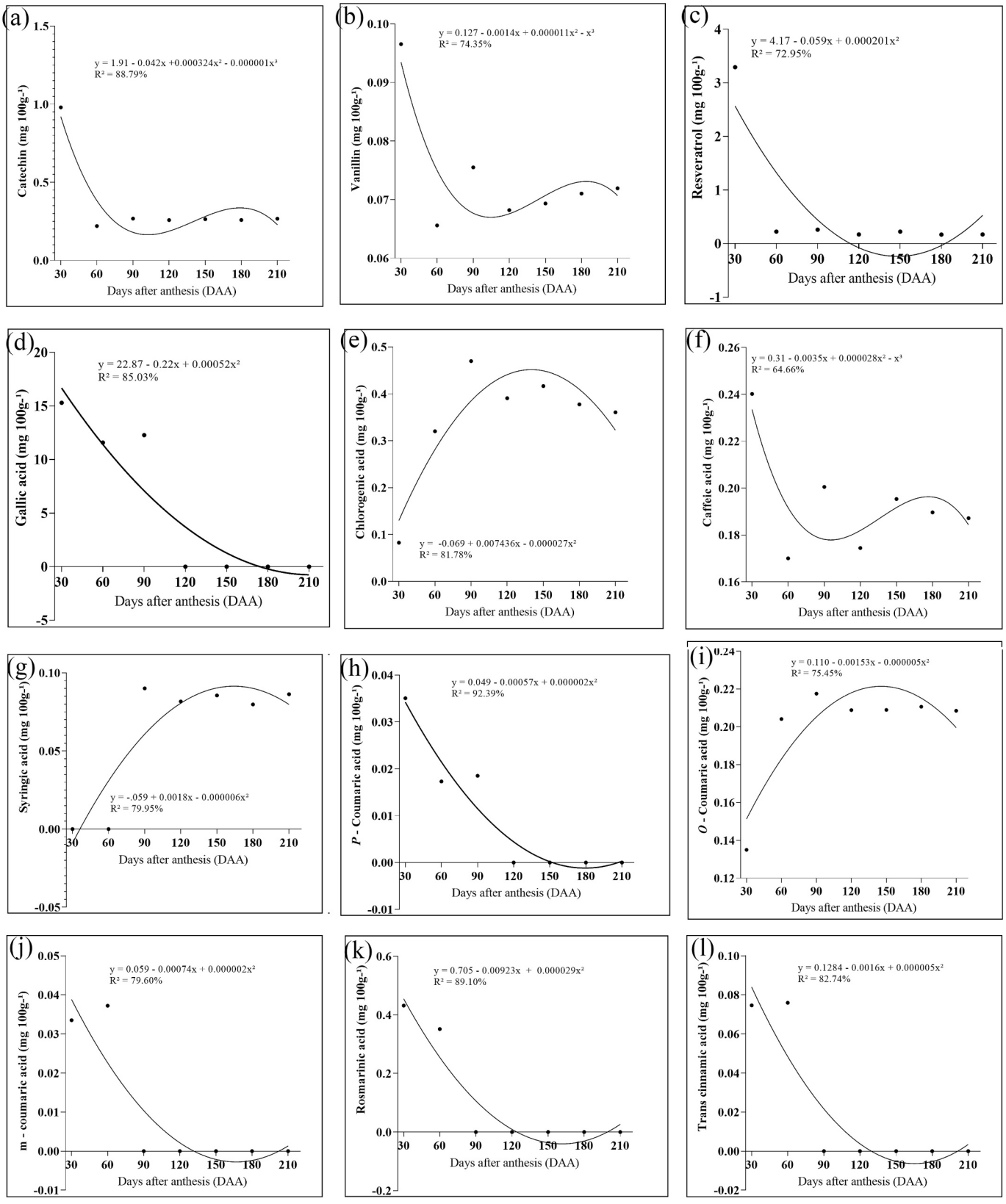

Fig. 4. Phenolic profile of *H. dulcis* pseudofruits during development.

3.2. Phenolic profile

In *H. dulcis* pseudofruits, twelve phenolic compounds were identified, comprising nine acids [gallic (GA), chlorogenic (CGA), caffeic (CaA), syringic (SA), *p*-, *m*-, and *o*-coumaric (*p*-, *m*-, and *o*-CuA), rosmarinic (RA), and *trans*-cinnamic (*t*-CiA)], one flavonoid (catechin), one stilbene (resveratrol), and one aldehyde (vanillin) (Fig. 4). CAT, VAN, RES, CGA, CaA, and *o*-CuA were identified throughout the entire developmental period, unlike the other compounds. SA was identified only from 120 and 90 DAA, respectively, while the presence of GA and p-CuA was limited to 30, 60, and 90 DAA, and *m*-CuA, RA, and *t*-CiA were limited to 30 and 60 DAA.

Among the identified phenolic compounds, GA was the most abundant component, although present only in the early stages of development, with concentrations ranging from 11.60 to 15.30 mg 100 g^{-1} (Fig. 4d). The high concentration of GA at 30 DAA, followed by its complete disappearance after 90 DAA, suggests a strong metabolic flux through the phenylpropanoid pathway and its derivatives in young tissues, likely acting as a chemical defense against herbivory during early development (Singh et al., 2017). The remaining phenolics were quantified at concentrations below 1 mg 100 g^{-1}, except for RES at 30 DAA (3.3 mg 100 g^{-1}) (Fig. 4). The presence of these compounds, even at low concentrations, reinforces the metabolic complexity and functional profile of the pseudofruits, in permanent change throughout development.

The sharp reduction in the concentrations of CAT, VAN, RES, and CaA observed between 30 and 60 DAA chronologically coincides with the progressive increase in pseudofruit firmness, which reaches its peak at 90 DAA (Fig. 2k). From a biochemical perspective, this simultaneous behavior suggests that the reduction of these free phenolic compounds did not result from degradation, but the rerouting of their metabolic precursors in the phenylpropanoid pathway toward the synthesis of structural polymers, such as lignin (Vogt, 2010). This intense initial lignification acts by cementing the cellulose and hemicellulose matrix, which justifies the hardening and firmness gain of the young tissue. In contrast, the stabilization of these phenolics at basal levels after 60 DAA and the subsequent decline in firmness, starting from 120 DAA, mark the end of this structural deposition phase and the beginning of the hydrolytic softening processes typical of fruit ripening. On the other hand, an increase in the concentrations of CGA and *o*-CuA were observed from 30 to 90 DAA, also followed by relative stabilization. The temporary accumulation of CGA may be associated with a physiological response of protection against oxidative stress (Rashidi et al., 2022), generated by the high metabolic rates typical of the transition period between cell division and expansion.

The SA, which was identified only starting at 90 DAA, and *p*-CuA, *m*-CuA, RA, and *t*-CiA, identified only in the early stages of development, remained relatively stable at low concentrations, fluctuating around 0.09, 0.02, 0.037, 0.35, and 0.076 mg 100 g^{-1}, respectively. Although present in small amounts, these metabolites may act as biosynthetic intermediates or in maintaining tissue redox balance. The restricted detection of compounds such as *p*-CuA and *t*-CiA to the early phases reinforces their role as active intermediates of the phenylpropanoid pathway, which are rapidly consumed and incorporated into matrices of greater macromolecular complexity of the cell wall (Vanholme et al., 2019) as the pseudofruit advances in its ontogeny, besides undergoing a natural physical dilution effect due to the volumetric expansion of the tissue.

The levels of CAT and RES dropped from 0.97 and 3.3 mg 100 g^{-1} to 0.26 and 0.17 mg 100 g^{-1} in immature green (30 DAA) and ripe (210 DAA) pseudofruits, respectively. The average CAT observed in ripe pseudofruits was lower than those reported for ripe fruits of *P. edulis* (0.6 mg 100 g^{-1}), *A. crassiflora* (7.99 mg 100 g^{-1}), and *C. brasiliense* (4.2 mg 100 g^{-1}) (Da Costa et al., 2023; Da Costa et al., 2024; Da Costa, Silva, et al., 2025), as was the RES content compared to that reported for ripe fruits of *C. brasiliense* (0.66 mg 100 g^{-1}) (Da Costa et al., 2024). Both compounds, CAT and RES, are synthesized from the fusion of *p*-coumaroyl-CoA (derived from the phenylpropanoid pathway) with three molecules of malonyl-CoA, through the action of chalcone synthase (CHS) and stilbene synthase (STS), respectively (Hasan & Bae, 2017; Yao et al., 2025). These differences reflect specificities in enzymatic regulation. For example, the highly branched nature of the catechin biosynthetic pathway (Zheng et al., 2014) may justify the variability observed in the ontogeny of *H. dulcis*. As the enzymes CHS and STS compete for the same precursor (*p*-coumaroyl-CoA), the drastic reduction of both compounds toward ripening suggests a downregulation of these specific branches or a redirection of the carbon flux toward the synthesis of cell wall polymers. On the other hand, the reduction of resveratrol throughout ripening suggests metabolic redirection or its consumption in defense mechanisms and redox protection during the early stages (Hasan & Bae, 2017). Besides its physiological function, resveratrol is recognized for its therapeutic potential in combating inflammation, diabetes, and cardiovascular and neurodegenerative pathologies (Berretta et al., 2020). Catechins, in turn, offer various health benefits, including the ability to prevent and reduce skin damage, high antioxidant activity, UV protection, as well as antimicrobial, anti-allergic, anti-inflammatory, antiviral, and anticancer properties (Bae et al., 2020).

The maximum CGA content was observed at 90 DAA (0.46 mg 100 g^{-1}), declining to 0.36 mg 100 g^{-1} in the ripe pseudofruit (Fig. 4e). This behavior resembles that observed by Wang et al. (2023) when studying apple (*Malus domestica*) cultivars throughout development. According to these authors, CGA peaks occurred in the early stages of development, although concentrations subsequently decreased to basal levels. The intermittent action of key enzymes, such as hydroxycinnamoyl-CoA shikimate/quinate hydroxycinnamoyl transferase (HCT) and *p*-coumarate 3-hydroxylase (C3H), coordinates CGA metabolism, responding to biotic and abiotic stresses, including light radiation, thermal variations, and phytohormone signaling (Soviguidi et al., 2022). Therefore, these factors may have influenced the changes in CGA levels observed during the development of *H. dulcis* pseudofruits, suggesting that the peak at 90 DAA represents an active physiological response for cellular protection. CGA, the condensation product of caffeic and quinic acids, is present in coffee beverages and, more generally, in fruits and vegetables. This phenolic has attracted attention due to its antioxidant, anti-inflammatory, and antimicrobial activities, besides its role in regulating lipid and glucose metabolism, which can be explored in therapies focused on the management of type 2 diabetes and cardiovascular diseases (Yu et al., 2022).

Contrary to the observations for CGA, but similarly to those of CAT and RES, the levels of CaA and VAN decreased when comparing immature green (30 DAA) and ripe (210 DAA) pseudofruits (Fig. 4b and f). CaA levels reduced from 0.24 to 0.19 mg 100 g^{-1}, while VAN levels dropped from 0.097 to 0.07 mg 100 g^{-1}. CaA values are lower than those reported for *A. crassiflora* (0.99 mg 100 g^{-1}) (Da Costa, Nascimento, et al., 2025) and *C. pubescens* (0.55 mg 100 g^{-1}) (Machado et al., 2025). CaA, commonly found in coffee beverages, exhibits various biological activities described by Yazar et al. (2025) in their extensive literature review: antioxidant, anti-hyperallergic, antimicrobial, anticancer, cytotoxic, anti-inflammatory, anticoagulant, and antidiabetic. In turn, VAN, a volatile phenolic aldehyde responsible for the characteristic aroma of vanilla, is extracted mainly from the seed pods of *Vanilla planifolia* and is widely used by the food and cosmetic industries.

A behavior contrary to that of CaA and VAN was observed for *o*-CuA, whose concentrations rose from 0.13 to 0.21 mg 100 g^{-1} in immature green (30 DAA) and ripe (210 DAA) pseudofruits, respectively (Fig. 4i). These values are higher than those observed in passion fruit pulp (0.06 mg 100 g^{-1}) (Da Costa et al., 2023).

The presence of the phenolic compounds GA, *p*-CuA, *m*-CuA, RA, and *t*-CiA exclusively in the early stages of development (Fig. 4d, h, j, k, l) may be associated with the intense initial activity of the general phenylpropanoid pathway enzymes (such as PAL and C4H) for the

protection of young tissues against biotic and abiotic stresses, as suggested by Li et al. (2023). On the other hand, the disappearance of these compounds may be linked to their direct utilization as building blocks in the synthesis of structural polymers, such as lignin and complex flavonoids, during the ripening process. Furthermore, the rapid expansion of the tissue promotes a physical dilution effect, reducing concentrations to levels below the analytical detection limit (Zhang et al., 2022).

SA was identified only starting at 90 DAA, fluctuating around 0.075 mg 100 g^{-1} up to 210 DAA. SA is a phenolic compound found in various fruits and vegetables, such as olives, dates, grapes, acai, and pumpkin; it exhibits antioxidant, antimicrobial, anti-inflammatory, anticancer, and antidiabetic activities, as well as protective effects on the heart, liver, and brain, while also contributing to the structural integrity of lignin (Srinivasulu et al., 2018). Since SA is a dimethoxylated derivative of GA, the appearance of the former starting at 90 DAA may be metabolically associated with the consumption and disappearance of the latter starting at 120 DAA, indicating an active late methylation pathway.

The results reveal that *H. dulcis* pseudofruits possess a phenolic profile that varies qualitatively and quantitatively throughout development. The phenolic compounds confirm this pseudofruit as a metabolically active vehicle with relevant antioxidant and functional potential. These findings consolidate *H. dulcis* pseudofruits as a plant matrix with significant nutritional and bioactive value, although poorly explored, while providing essential bases regarding the biochemical and enzymatic mechanisms that regulate its development.

3.3. Volatile organic compounds (VOCs)

Volatile compounds play a fundamental role in the aroma and sensory acceptance of food products. In *H. dulcis* pseudo-ruits, 25 volatile compounds were identified (Table 1), showing significant variations throughout development ($p < 0.05$). Chemical characterization was performed by comparing mass spectra with Wiley 8 and NIST libraries, adopting a similarity index ≥80% for identity confirmation. The identified compounds were classified into eight chemical categories, with a predominance of alcohols (32%) and terpenes (16%), followed by aldehydes, esters, terpene oxides, acids, ketones, and hydrocarbons (Table 1). Both the concentration and the profile of these constituents

Table 1
Volatile organic compounds identified in *H. dulcis* pseudofruits during development.

Classe Química	Compound	RI Calc	RI Lit	Odor	Area (%) S1	Area (%) S2	Area (%) S3	Area (%) S4	Area (%) S5	Area (%) S6	Area (%) S7
Alcohols	2.3-Butanediol	806	806	fruit. Onion	–	–	–	–	–	–	1 ± 0.01
	(*Z*)-3-hexenol	854	858	grass	1 ± 0.13^{a}	0.75 ± 0.03^{d}	0.40 ± 0.1^{f}	0.96 ± 0.07^{b}	0.8 ± 0.07^{c}	0.53 ± 0.01^{e}	–
	(*E*)-2-hexen-1-ol	864	853	green. Leaf. walnut	0.41 ± 0.07^{a}	–	0.16 ± 0.00^{b}	–	–	–	–
	1-hexanol	867	863	resin. Flower. green	3.29 ± 0.22^{g}	4.37 ± 0.41^{f}	11.96 ± 0.7^{d}	22.68 ± 1.3^{c}	35.97 ± 1.6^{b}	43.82 ± 2.7^{a}	6.9 ± 0.08^{e}
	2-heptanol	902	894	mushroom	52.79 ± 2.1^{a}	41.3 ± 2.91^{b}	31.63 ± 2.5^{c}	15.85 ± 0.8^{d}	9.14 ± 0.84^{e}	6.83 ± 0.18^{f}	4.63 ± 1.1^{g}
	1-octen-3-ol	980	982	mushroom	–	–	–	1.14 ± 0.11^{b}	0.8 ± 0.00^{c}	0.49 ± 0.01^{d}	1.31 ± 0.13^{a}
	Lavanduol	1165	1165	herb	0.81 ± 0.14^{a}	0.11 ± 0.03^{b}	–	–	–	–	–
	Borneol	1175	1165	camphor	0.86 ± 0.09^{b}	0.11 ± 0.02^{c}	1.67 ± 0.05^{a}	–	–	–	–
Terpenes	Camphene	950	953	camphor	0.11 ± 0.04	–	–	–	–	–	–
	Myrcene	989	988	balsamic. Must. pice	–	0.01 ± 0.01	–	–	–	–	–
	Limonene	1030	1030	citrus. Mint	1.98 ± 0.45^{b}	1.74 ± 0.42^{c}	3.19 ± 0.17^{a}	0.81 ± 0.04^{e}	0.29 ± 0.03^{f}	1.04 ± 0.05^{d}	–
	(Z)-ocimene	1047	1043	citrus. Herb. flower	2 ± 0.16^{a}	0.08 ± 0.04^{b}	–	–	–	–	–
Aldehydes	Hexanal	801	801	grass. Tallow. fat	2.41 ± 0.04^{e}	7.94 ± 0.75^{a}	4.81 ± 0.21^{c}	4.22 ± 0.62^{d}	2.04 ± 0.23^{f}	7.34 ± 0.18^{b}	0.21 ± 0.01^{g}
	(E)-2-hexenal	850	844	green. Leaf	1.6 ± 0.1^{b}	2.36 ± 0.37^{a}	–	0.87 ± 0.06^{d}	0.25 ± 0.02^{e}	1.17 ± 0.05^{c}	–
	Benzaldehyde	964	960	almond. Burnt sugar	–	–	–	–	–	–	0.57 ± 0.09
Esters	Ethyl isovalerate	850	849	apple. Pear	–	–	–	–	–	–	0.21 ± 0.00
	Ethyl hexanoate	998	997	apple peel. Fruit	–	–	–	–	–	–	0.15 ± 0.05
Terpene oxides	Methyl salicylate	1195	1190	peppermint	7.26 ± 0.55^{d}	19.3 ± 2.61^{c}	–	20.35 ± 2.1^{b}	20.39 ± 1.9^{a}	–	–
	1.8-cineole	1033	1030	mint. Sweet	0.63 ± 0.12^{a}	–	–	0.24 ± 0.07^{b}	–	–	–
	(E)-linalool oxide	1088	1084	flower	0.63 ± 0.03	–	–	–	–	–	–
Acids	Isovaleric acid	847	827	sweat. Acid. rancid	–	–	–	–	–	–	1.05 ± 0.11
	2-Methylbutanoic acid	853	873	cheese. Sweat	–	–	–	–	–	–	0.27 ± 0.03
Ketones	2-heptanone	888	889	soap	3.50 ± 0.31^{c}	2.38 ± 0.26^{e}	12.58 ± 0.2^{a}	3.95 ± 0.3^{b}	3.11 ± 0.09^{d}	1.98 ± 0.01^{f}	–
	3-Octanone	985	979	herb. Butter. resin	–	–	–	–	–	–	0.47 ± 0.13
Hidrocarbons	Styrene	892	892	balsamic. Gasoline	–	0.55 ± 0.14^{b}	1.41 ± 0.05^{a}	0.34 ± 0.02^{d}	–	0.38 ± 0.05^{c}	–

showed significant variations during development, reflecting an intense reprogramming of the secondary metabolism.

Values represent the mean and standard deviation. Results were expressed as a percentage of the total area. Different letters indicate significant differences ($p < 0.05$) by analysis of variance (ANOVA), followed by Tukey's test. ND: not detected; RI: calculated retention index; RI Lit: retention index found in the literature.

Alcohols constituted the predominant class of volatiles across all analyzed stages. Among them, 2-heptanol and 1-hexanol were the most abundant; the former showed higher concentrations in the early stages (30, 60, and 90 DAA), while the latter predominated in the final stages (120 to 210 DAA) (Table 1). Both compounds exhibited opposite kinetic profiles: 1-hexanol showed a progressive increase, whereas 2-heptanol demonstrated a linear decline during ripening. The increase in 1-hexanol levels is likely associated with the activation of the lipoxygenase (LOX) pathway, contributing to the expression of herbaceous sensory notes (Han & Barringer, 2016). Biologically, this phenomenon is attributed to the loss of cellular compartmentalization during ripening, which facilitates contact between LOX enzymes and their lipid substrates (polyunsaturated fatty acids), resulting in the biosynthesis of these volatiles (Bate & Rothstein, 1998). This process is corroborated by firmness loss data and SEM micrographs (Figs. 2k and 3). Furthermore, the decreasing behavior of 2-heptanol reinforces the metabolic relevance of this class in tropical fruits, analogous to observations in passion fruit maturation (Da Costa et al., 2023).

A clear metabolic reorganization of alcohols was observed, in which six-carbon (C6) defense volatiles such as (Z)-3-hexen-1-ol and (E)-2-hexen-1-ol, derived from the cleavage of fatty acid hydroperoxides by the enzyme hydroperoxide lyase (HPL) were restricted to the early stages (Zhou et al., 2021). As maturation progressed, these compounds gave way to volatiles of greater aromatic complexity, such as 1-octen-3-ol (characteristic of fungal/earthy notes) and 2,3-butanediol. This transition suggests a shift in metabolic investment: the plant reduces the synthesis of herbivory signals (Green Leaf Volatiles - GLVs) as the pseudofruit accumulates energy reserves. This hypothesis is supported by data for soluble solids, sugars, and starch (Figs. 2 j, p, q), where an increase in the former and a decline in the latter are observed, respectively. This profile indicates a transition toward a chemical phenotype that favors attractivity for dispersers, a pattern also validated by the phenolic metabolism (Fig. 4) discussed previously. Moreover, the presence of these alcohols in immature tissues is fundamental, as they serve as substrates for the subsequent synthesis of ripening-related volatile esters (Ortiz et al., 2011).

Changes in the volatile profile during development are further corroborated by the dynamics of terpenes and aldehydes. While limonene persisted throughout ontogeny, indicating continuous biosynthesis via the mevalonate (MVA) and methylerythritol phosphate (MEP) pathways for defense and attraction (Aharoni et al., 2006; Rosenkranz et al., 2021), other terpenes and C6 aldehydes, such as hexanal and (E)-2-hexenal, predominated only in the early stages. The reduction of these “green” aldehydes (Feussner & Wasternack, 2002) in favor of the late accumulation of benzaldehyde, which is typically floral (Lv et al., 2024), marks a sensory migration from an herbaceous profile to a floral bouquet at full maturity. The presence of benzaldehyde, a phenolic aldehyde derived from the phenylpropanoid pathway (shikimate pathway), is consistent with the detection of vanillin (4-hydroxybenzaldehyde) in the phenolic profile (Fig. 4d), evidencing metabolic coordination between soluble and volatile compounds.

Simultaneously, the consolidation of the mature pseudofruit's characteristic volatile profile is driven by the biosynthesis of esters, such as ethyl isovalerate and ethyl hexanoate. The exclusive detection of these compounds in the fully ripe stage (S7) (Table 1) suggests temporal enzymatic coordination, where the initial activity of alcohol dehydrogenases (ADH) provides the necessary substrates for alcohol acyltransferases (AAT) in the final phase (Qian et al., 2019), a pattern also observed in tropical fruits such as pequi (Da Costa et al., 2024). These data converge with results reported for ‘Golden Reinders’ apples, where the activity of these enzymes is directly related to the increase in esters during ripening. This reinforces that volatile ester production results, in part, from the increased availability of precursors, such as alcohols and acyl-CoA, for AAT action (Ortiz et al., 2011).

Finally, the minor volatile profile elucidates the physiological transition of the pseudofruits. The presence of terpene oxides restricted to the early stages, followed by the accumulation of isovaleric and 2-methylbutanoic acids at maturity, signals a metabolic shift toward the degradation of branched-chain amino acids (BCAAs), such as leucine and isoleucine. This transition reflects the intensification of catabolic processes and late oxidative activity (Bizzio et al., 2022). Similarly, the replacement of 2-heptanone by 3-octanone in the ripe stage reflects late metabolic events involving lipid degradation and membrane oxidation (El Hadi et al., 2013; Schwab et al., 2008). Taken together, these variations demonstrate that maturation in *H. dulcis* pseudofruits acts as the primary metabolic modulator, replacing primary defense mechanisms with an aromatic complexity aimed at palatability and seed dispersal.

3.4. Proteomics

In *H. dulcis* pseudofruits, approximately 496 proteins were identified across the seven developmental stages analyzed. Among these, 222 exhibited significant variations in abundance ($q < 0.1$ and FC > 2), with differences reaching up to 8781-fold between developmental stages (Supplementary Table 1). This subset of proteins showed the following abundance distribution per stage: 15 in stage S1, 3 in stage S2, 2 in stage S3, 31 in stage S4, 84 in stage S5, 33 in stage S6, and 54 in stage S7.

The identified proteins were classified into 30 functional categories, mostly associated with biological and metabolic processes (Fig. 5a). Due to their participation in multiple metabolic pathways and different cellular compartments, some proteins were linked to more than one biological process. Furthermore, Principal Component Analysis (PCA) (Fig. 5b), performed using the three replicates of the 496 proteins for each stage, demonstrated that the proteomic profiles of the replicates for each stage clustered consistently, evidencing high data reproducibility.

Functional enrichment analysis revealed that the proteins accumulated in *H. dulcis* pseudofruits are involved in 10 biological processes, with emphasis on those related to responses to temperature and abiotic stimuli (Fig. 4a). Complementarily, the KEGG pathway analysis (Fig. 5c) highlighted that central carbon metabolism was strongly impacted, notably carbon fixation in photosynthetic organisms and glyoxylate and dicarboxylate metabolism, which showed the highest levels of fold enrichment and statistical significance.

The processes with the highest number of proteins were biological processes (135) and metabolic processes (112). Among these, 56 proteins were selected based on their metabolic functions in the fruits, and a heatmap was generated to visualize their distribution and abundance (Fig. 6a).

The topological analysis of the protein-protein interaction network (Fig. 6b) revealed a scale-free architecture, characterized by the presence of critical structural proteins known as hubs. The TIM protein was identified as the primary central node of the system, exhibiting the maximum values for Degree (12.00) and Betweenness Centrality (0.14), as indicated by the node size scale and deep purple coloring, respectively. This centrality suggests that TIM plays an essential regulatory role in coordinating signaling flow between peripheral clusters. Proteins such as GAPC1, GAPC2, and MDH showed intermediate centrality values (approximately 0.07), acting as communication bridges between the central core and more specialized sub-networks, such as the cluster formed by CSD1, CSD2, and CAT2, which demonstrated lower topological dependence within the global context of the network.

3.4.1. Photosynthesis

Four isoforms of Rubisco (EC 4.1.1.39) were identified, three of which showed peak expression at stage 5 (S5), with an increase of up to

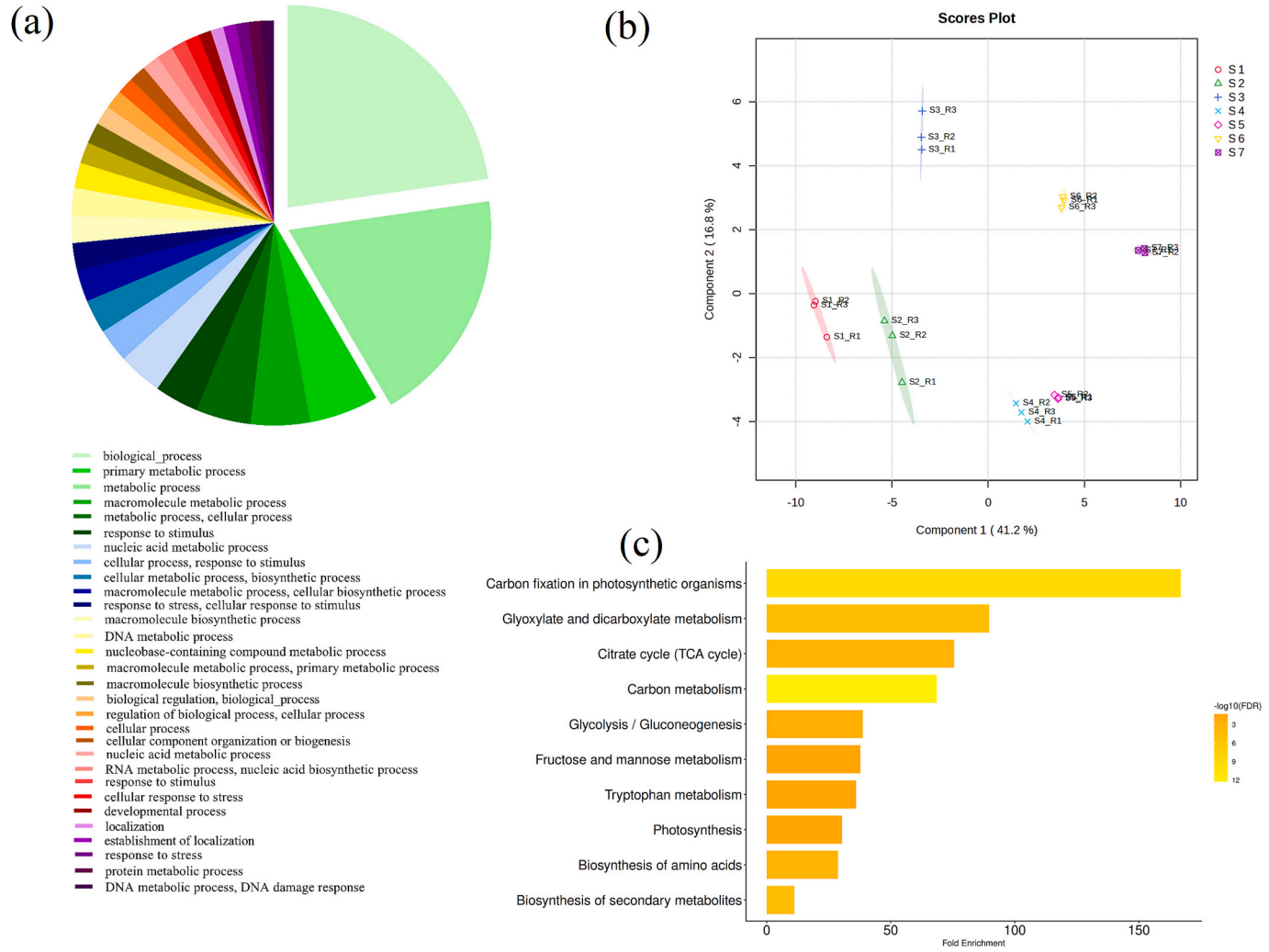

Fig. 5. Functional Annotation of biological processes (a), PCA (b), and Functional Enrichment Analysis of identified proteins based on the KEGG database (c) for differentially abundant proteins across the seven developmental stages (30 to 210 DAA) of *H. dulcis* pseudofruits.

632-fold (Fig. 6a, $q < 0.1$). Although fruits are primarily metabolic sinks, the presence of chlorophyll in the dermal tissue of *H. dulcis* pseudofruits supports a local photosynthetic capacity. The exacerbated expression of Rubisco at the onset of ripening (S5) suggests that photosynthesis within the pseudofruit itself provides essential ATP, NADPH, and carbon skeletons for metabolite biosynthesis and the intense sugar accumulation observed (Fig. 2o; Garrido et al., 2023). This endogenous activity reinforces the enzyme's role in assisting the synthesis of starch and storage compounds during the metabolic transition to ripening (Jiang et al., 2020).

Photosystems I and II (PSI and PSII) are the primary components of the electron transfer process, playing a fundamental role in converting absorbed energy into chemical energy during photosynthesis (Rane et al., 2021). In the analyzed pseudofruits, specific enzymatic isoforms for PSI and PSII were identified, showing higher expression at stages S4 and S6, respectively. Consequently, these results suggest an increase in photosynthetic activity within the pseudofruits during these developmental stages. These increases may be associated with the rise of seven Rubisco isoforms in S5, the enzyme responsible for carbon fixation in the photosynthetic process.

One isoform of triose phosphate isomerase (TPI, EC 5.3.1.1) and another of phosphoglycerate kinase (PGK, EC 2.7.2.3) were identified in the studied pseudofruits, showing higher expression at stage S5 (Fig. 6a), coinciding with the peak expression of Rubisco and reinforcing the synchrony in carbon metabolism. TPI and PGK are fundamental for the interconversion of triose phosphates produced in the Calvin cycle, ensuring energy homeostasis and the carbon supply for the biosynthesis of metabolites essential for development (Li et al., 2014).

This enzymatic coordination suggests that, at S5, the pseudofruit prioritizes the partitioning of trioses toward the formation of organic matter and reserves. Conversely, the decline in the expression of TPI, PGK, and Rubisco in the final stages (S6 and S7) signals a reduction in autotrophic activity and primary metabolism at the peak of maturity. Understanding these local photosynthetic dynamics in fruits is strategic for genetic improvement and the management of microenvironmental conditions aiming at productivity and quality (Garrido et al., 2023).

3.4.2. Glycolysis: Glyceraldehyde-3-phosphate dehydrogenase and pyruvate kinase

Six isoforms of Glyceraldehyde-3-phosphate dehydrogenase (GAPDH, EC 1.2.1.12) showed significant variations in expression throughout the cycle (Fig. 6a), suggesting a regulatory role in the development of *H. dulcis* pseudofruits (Choi et al., 2022). The oscillation of these isoforms reflects the metabolic adaptation of tissues to the energetic and biosynthetic demands of the pseudofruit. Depending on the stage, GAPDH can act both in the glycolytic flux for energy generation and in the gluconeogenic pathway for starch and sugar synthesis, highlighting its importance in carbon partitioning during ripening (Luo et al., 2020).

Two isoforms of pyruvate kinase (PK, EC 2.7.1.40) were identified in

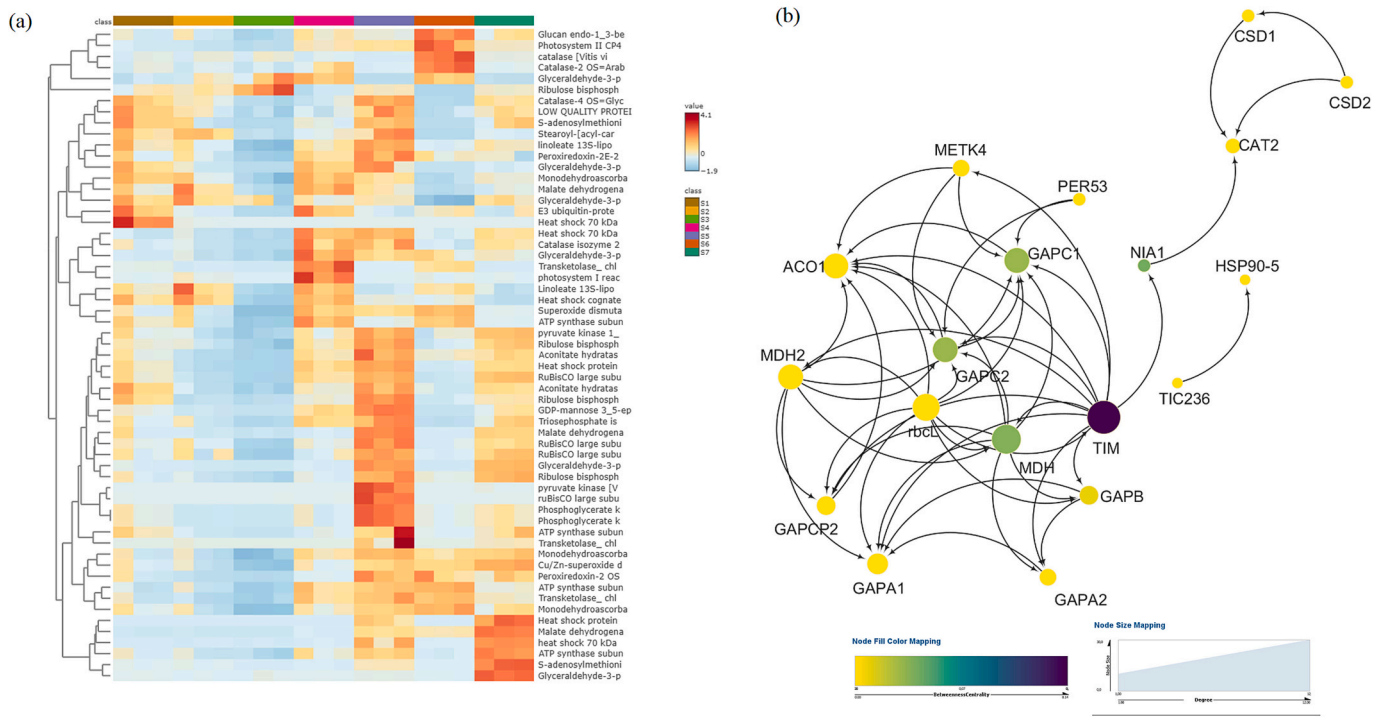

Fig. 6. (a) Heatmap of differentially abundant proteins and (b) Protein-Protein Interaction (PPI) network with mapping of Degree and Betweenness Centrality parameters.

the pseudofruits of the Japanese raisin tree, with higher expression at S5 and lower expression during the early developmental stages (S1 and S3) (Fig. 6a). PK catalyzes the conversion of phosphoenolpyruvate (PEP) to pyruvate, generating ATP, making it an essential enzyme in the final step of glycolysis (Ambasht & Kaystha, 2002). Its lower expression in early stages compared to S5 suggests an intensification of glycolysis at the onset of ripening, a period of high energy demand. Conversely, its lower expression in the initial stages may indicate that, during this period, energy metabolism may rely on other pathways, such as the pentose phosphate pathway, as well as mitochondrial oxidative phosphorylation based on lipids and/or amino acids.

3.4.3. *Pentose phosphate pathway*

Three isoforms of transketolases (TK, EC 2.2.1.1) were identified in the pseudofruits, with higher expression at S5 and lower expression during the early developmental stages (S1 and S3) (Fig. 6a). TK is the primary regulatory enzyme of the non-oxidative branch of the pentose phosphate pathway, playing a fundamental role in the interconnection between this pathway and glycolysis, in addition to being essential for the synthesis of coenzymes, vitamins, and nucleotide precursors (Kochetov & Solovjeva, 2014). Its higher expression at S5 supports the previously presented data, suggesting an increase in energy demand at the onset of ripening.

3.4.4. *Krebs cycle and oxidative phosphorylation*

Two isoforms of aconitate hydratase (also known as aconitase, EC 4.2.1.3) were identified in the pseudofruits, showing higher expression at S5 and lower at S3 (Fig. 6a). These enzymes are responsible for the reversible isomerization of citrate to isocitrate via the cis-aconitate intermediate (Yun et al., 2010). Furthermore, aconitase can regulate the carbon flux between organic acid and sucrose metabolism (Carrari et al., 2003). As the fruit ripens, the conversion of organic acids may be reduced, leading to sugar accumulation. The activity of this enzyme may be a regulatory factor in this process, which is supported by the change in acidity of the analyzed pseudofruits (Fig. 2m).

Three isoforms of malate dehydrogenase (MDH, EC 1.1.1.37) exhibited peak expressions at S4, S5, and S7 (Fig. 6a). Although MDH acts in the interconversion of oxaloacetate into malate, a central component of sensory quality (Yao et al., 2011), its high expression did not follow the same proportion as the titratable acidity (Fig. 2m). This divergence indicates that malate dynamics in *H. dulcis* are governed by complex multigenic control, where MDH may act in both the synthesis and oxidation of the acid to supply other metabolic pathways, as observed in apples (Zhang et al., 2022).

Five isoforms of ATP synthase (EC 3.6.3.14) were identified, with maximum expression fluctuating between stages S4 and S7 (Fig. 6a). Responsible for the final step of oxidative phosphorylation (Liu et al., 2021), the variation of this enzyme reflects the fluctuations in cellular energy supply required to regulate ripening and senescence (Wang et al., 2013). Systemically, the abundance profile of enzymes from the Calvin cycle, glycolytic pathways, and the Krebs cycle confirms that the onset of ripening (S5) is the stage of highest energetic and biosynthetic demand in *H. dulcis* pseudofruits.

3.4.5. *Stress, defense, and antioxidant system*

Fruits are dynamically exposed to stress factors that trigger defense mechanisms, typically associated with antioxidant systems. Superoxide dismutase (SOD, EC 1.15.11) constitutes the first line of defense against reactive oxygen species (ROS), rapidly converting them into H_2O_2 and O_2 (Gill et al., 2015). Two SOD isoforms were identified, showing higher expression in the final developmental stages (S6 and S7) and lower expression in S3 (Fig. 6a). The increased expression of this enzyme in the final stages of the pseudofruit of the Japanese raisin tree is consistent with the greater accumulation of free radicals that occurs during senescence. Therefore, SOD action is vital for free radical scavenging and combating aging. Indeed, SOD expression is an indicator that the plant is likely employing antioxidant mechanisms to protect its cells (Masia, 1998).

Due to its toxic nature, the H_2O_2 produced by SOD or other mechanisms must be eliminated. Thus, Catalase (CAT, EC 1.11.1.6) is a highly expressed enzyme, especially in specific plant cell types, and plays a fundamental role in the plant antioxidant system (Mhamdi et al., 2010).

Its primary function is to eliminate H_2O_2 generated during mitochondrial electron transport, fatty acid oxidation, and, most importantly, photorespiration, under both normal and stress conditions (Sharma & Ahmad, 2014). In the analyzed pseudofruits, four catalase isoforms were identified; two showed higher expression at stages S4 and S5, while the other two were more expressed in S6 (Fig. 6a). These patterns suggest a dynamic response to oxidative stress throughout development. Their expression at these stages may be linked to intense metabolic changes, adaptation to environmental stress, ripening and senescence processes, or defense against biotic stresses (Masia, 1998; Rodrigues-Ruiz et al., 2019).

Peroxiredoxin 2 (Prx2, EC 1.11.1.15) is an antioxidant enzyme that utilizes cysteine residues to decompose peroxides. In the analyzed pseudofruits, two isoforms of this enzyme were identified, with peak expression observed at stage S5 and the lowest at S3 (Fig. 6a). The difference in expression between these stages exceeds 150-fold, highlighting significant variation in Prx2 regulation during development. These results suggest a possible increase in ROS production or a link to physiological ripening processes, such as changes in cellular respiration, pigment synthesis, and alterations in secondary metabolism.

Heat shock proteins (HSPs) are highly conserved across living organisms throughout evolution. Although structurally related, they perform distinct functions within the cell. Several HSPs can coexist in a single cell, distributed across compartments such as the endoplasmic reticulum, mitochondria, and cytosol (Tutar & Tutar, 2011). In the analyzed pseudofruits, six isoforms were identified: four belonging to the HSP70 family, one to the HSP80 family, and two to the HSP90 family (Fig. 6a). These isoforms showed significant variations in expression between stages S1, S4, S5, and S7. These results suggest that, during development, the pseudofruits were exposed to thermal stress, likely associated with temperature variations. Additionally, stress factors such as drought, high irradiation, salinity, or other abiotic stresses can interfere with HSP expression (Al-Whaibi, 2011), justifying the observed variations in the Japanese raisin tree pseudofruits.

Another protein related to biotic and abiotic stress signaling found in *H. dulcis* pseudofruits was E3 ubiquitin ligase (EC 2.3.2.27). One isoform of this protein was identified, with higher expression at stage S1 (Fig. 6a). This may indicate an early response to stress or preparation for future physiological demands related to development and environmental stress (Mao et al., 2022).

3.4.6. Vitamin C

One isoform of GDP–mannose 3,5-epimerase (GME, EC 5.1.3.18) was identified in the Japanese raisin tree pseudofruits, showing higher expression at S5 and lower at S3. This enzyme is crucial in the reversible conversion of GDP-D-mannose to GDP-L-galactose (Celi et al., 2023; Smirnoff et al., 2001) within the synthesis pathway of 2,3-enediol-L-gulonic acid, commonly known as vitamin C or ascorbic acid (AA). This pathway, known as the D-mannose/L-galactose or Smirnoff-Wheeler pathway, is recognized as the most likely route for AA production in plants (Smirnoff et al., 2001). The lower expression at S3 follows the initial decline of vitamin C occurring at S2 and extends until S4 (Fig. 2q). The peak expression at S5 coincides with the rise in vitamin C between S4 and S5 (Fig. 2q). These results reinforce the role of GME in vitamin C biosynthesis.

In addition to its important role in AA synthesis, GME also acts in the synthesis of cell wall compounds. Indeed, the GDP-L-galactose produced from GDP-D-mannose by GME is used not only for vitamin C production but also in the biosynthesis of glycoproteins and cell wall polysaccharides, playing an essential role in plant development (Smirnoff et al., 2001; Wang et al., 2015).

The AA produced by plants is recognized for its specific function in redox reactions in response to oxidative stress (Celi et al., 2023). Through the action of ascorbate oxidase or ascorbate peroxidase, it is oxidized to monodehydroascorbic acid (MDHA) and dehydroascorbic acid (DHA), and is regenerated back to AA by the enzymes MDHA reductase and DHA reductase, using glutathione and NADPH + H^+ as reducing agents (Noctor & Foyer, 1998).

Three isoforms of MDHA reductase (MDHAR, EC 1.6.5.4) were found in the pseudofruits of the Japanese raisin tree, with the highest expression occurring at developmental stages S4, S5, and S6, and the lowest at stage S3 (Fig. 6a). Over the same interval, a variation in vitamin C content was observed (Fig. 2q), suggesting the involvement of this enzyme in ascorbic acid regeneration in response to oxidative stress in the Japanese raisin tree pseudofruits.

3.4.7. Ethylene

In the analyzed pseudofruits, two isoforms of S-adenosylmethionine synthase (SAMS, EC 2.5.1.6) were identified (Fig. 6a), showing peak expression at developmental stages S5 and S7, with a 340-fold increase compared to stage S3, which exhibited the lowest enzyme expression. SAMS plays a fundamental role in ethylene biosynthesis, catalyzing the conversion of L-methionine and ATP into S-adenosylmethionine (SAM), an essential intermediate in general cellular metabolism. SAM serves as a precursor for polyamines during the juvenile phase of fruits, as well as for 1-aminocyclopropane-1-carboxylic acid (ACC), which subsequently gives rise to ethylene, the fruit ripening hormone (Machado et al., 2025). It also acts as a donor of methyl groups essential for the metabolism of various plant organs. Thus, the increase in SAMS expression in the final stages of development suggests its role in ethylene synthesis and the ripening of the Japanese raisin tree pseudofruits, as well as in the methylation of metabolites, such as pectic substances.

3.4.8. B-glucans

In the pseudofruits under study, an isoform of the enzyme Glucan β (1–3) glucosidase (GBG) was identified, with peak expression at stage S6. GBGs, classified as *endo*-β (1–3) glucanases (EC 3.2.1.39) and exo β (1–3) glucanases (EC 3.2.1.58), catalyze the hydrolysis of β (1–3) glycosidic bonds in β (1–3) -D-glucans (Ramos & Malcata, 2010). This enzyme acts in cell wall degradation, and its levels increase significantly during the defense process against fungal pathogens (Kebede & Kebede, 2021). *H. dulcis* is recognized as a vehicle for polysaccharides, whose presence has been associated with the hypoglycemic effects of the pseudofruit (Zhu et al., 2025). Therefore, the presence of an isoform of this enzyme supports its potential depolymerizing activity in mature fruits. The peak activity of GBG at S6 may be associated with the decline in pseudofruit firmness between S6 and S7, given that β (1–3) glucans are considered cell wall polysaccharides.

3.5. Principal component analysis (PCA) and hierarchical cluster analysis (HCA)

The results of the physicochemical, metabolic, and proteomic analyses of *H. dulcis* pseudofruits across seven developmental stages were subjected to multivariate analysis, performed considering the 53 most significant variables (top features), where PC1 and PC2 cumulatively explain 64.8% of the total data variation (40.2% and 24.6%, respectively; Fig. 7a). Considering a loading cutoff of 0.02 (Supplementary Table 2), the variables responsible for the separation in PC1 were: PSII, TPI, PGK, GAPDH, PK, TK, aconitate hydratase, MDHs, CAT, HSPs (70, 82, 90–5), E3 ubiquitin, Prx2, SOD, linoleate lipoxygenase, MDHAR, GME, SAMS, GBG, isovaleric acid, 2-methylbutanoic acid, 1-hexanol, benzaldehyde, 1-octen-3-ol, 3-octanone, ethyl hexanoate, *o*-CuA, mass, density, soluble pectin, total pectin, pH, sugar, anthocyanins, starch, and soluble solids. In fact, the visual analysis of Fig. 7a confirms that these compounds are associated with developmental stages S4 to S7, situated opposite to RuBisCO, stearoyl-desaturase, hexanal, (*E*)-2-hexenal, (*Z*)-3-hexenol, (E)-2-hexen-1-ol, 2-heptanone, styrene, 2-heptanol, camphene, limonene, 1,8-cineole, (Z)-ocimene, (E)-linalool oxide, lavandulol, borneol, methyl salicylate, GA, CAT, CGA, CaA, VAN, *p*-CA, RES, L*, C*, h°, TA, Vit C, total carotenoids, total chlorophyll, and firmness, which characterize the fruits in stages S1 to S3.

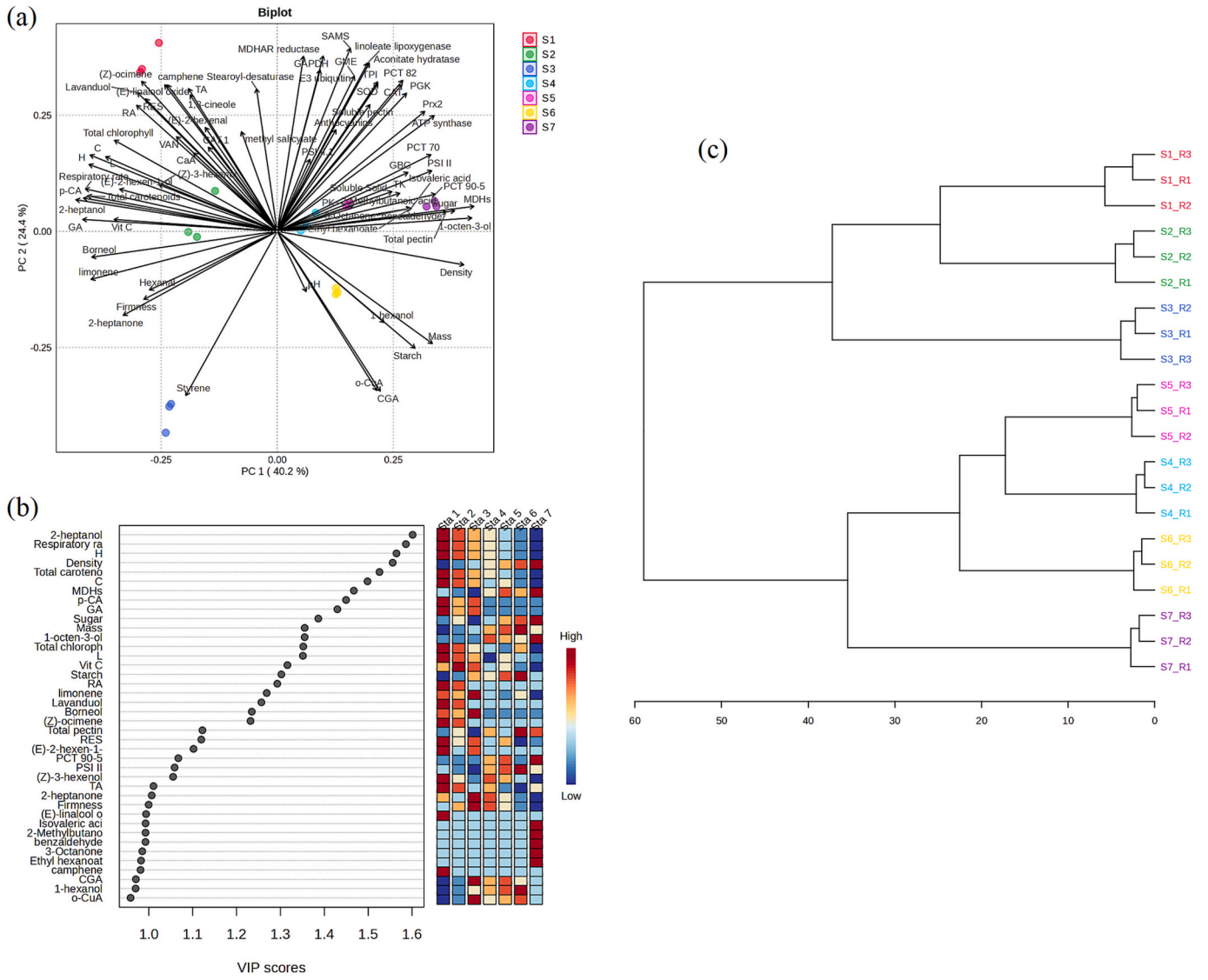

Fig. 7. (a) Biplot (PCA), (b) Variable Importance in Projection (VIP Score), and (c) Hierarchical Cluster Analysis (HCA) dendrogram.

The VIP (Variable Importance in Projection) score analysis (Fig. 7b) identified that the metabolic transition during the ripening of *H. dulcis* is primarily governed by changes in the volatile profile (2-heptanol) and respiratory physiology. The high VIP values for density and Hue angle (h°) corroborate the observed physical transformations; statistically, these variables showed high loadings on Comp 1, establishing themselves as the most discriminating phenological events between stages. Furthermore, the activity of the malate dehydrogenase (MDH) enzyme contributed significantly to this separation, reinforcing the reorganization of central metabolism during pseudofruit development.

Hierarchical Cluster Analysis (HCA, Fig. 7c) corroborated the PCA and sPLS-DA results (Figs. 7a and b), segmenting the samples into two main clusters: the first, grouping the early stages (S1 to S3) and the second encompassing all stages of maturation, including ripening (S4 to S7). This separation is supported by the sign inversion in the loadings of variables such as starch and biomass (mass) relative to phenolic compounds (*p*-CA, GA), marking a profound metabolic transition starting from stage S4. The high similarity between biological replicates reinforces the robustness of the obtained proteomic and metabolic profiles.

3.6. *Multi-omics integration: Correlations between proteins and metabolites*

Pearson correlation analysis (Fig. 8, Supplementary Table 3) reinforced the covariance structure observed in the PCA, allowing for the identification of specific associations at the molecular level. A broad spectrum of coefficients was observed, ranging from negligible associations to extremely strong correlations ($r > 0.99$; $p < 0.05$), such as those verified between the metabolites 2-methylbutanoic acid and isovaleric acid, and between *p*-CA and GA. These correlations suggest metabolic co-regulation or enzymatic regulation, validating the integration of the proteomic and metabolic datasets.

The results reveal a highly coordinated system between energy metabolism, antioxidant defenses, and cell wall restructuring during pseudofruit development. Central metabolism acted as the primary integration axis for the datasets. The GAPDH enzyme stood out due to an extremely strong coupling (r > 0.9) with MDHAR, SAMS, and linoleate lipoxygenase, suggesting that glycolytic flux is intrinsically linked to ethylene signaling and redox responses. Complementarily, TPI and PGK showed strong ($r > 0.7$) to very strong (r > 0.9) correlations with ATP synthase, aconitate hydratase, and Prx2, indicating a rigorous synchrony between energy production (ATP) and the neutralization of reactive oxygen species generated by respiratory metabolism. MDHs exhibited a

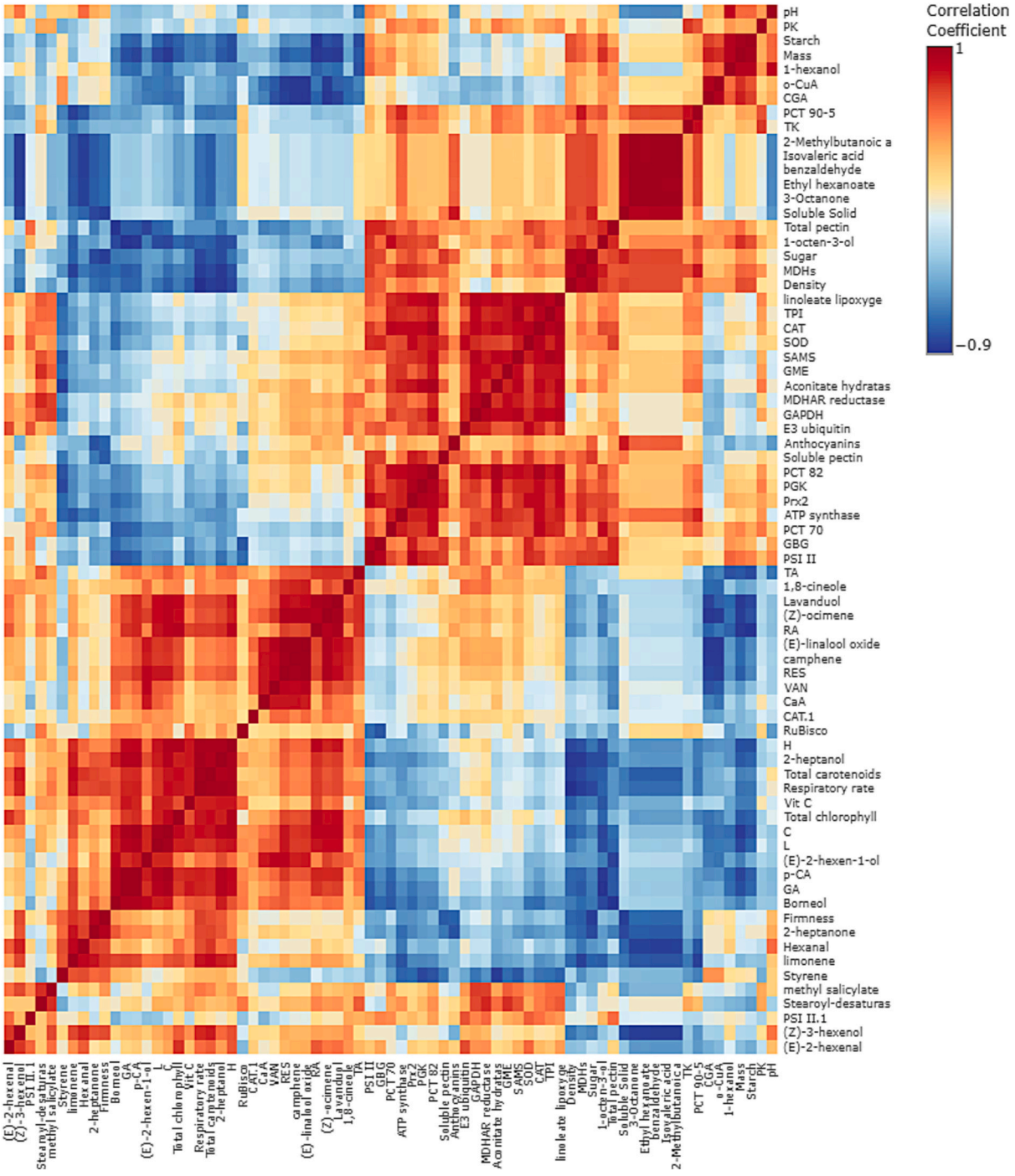

Fig. 8. Pearson correlation matrix between physicochemical variables, metabolites, and proteins during the ripening of *H. dulcis* pseudofruits.

very strong correlation ($r > 0.9$) with density and sugar content, as well as moderate associations with various volatiles (isovaleric and 2-methylbutanoic acids), consolidating their role in flavor transition and biomass accumulation.

Proteins of the photosynthetic apparatus showed correlations marking the decline of autotrophy and the progression of programmed senescence. Rubisco correlated moderately ($r > 0.5$) with vitamin C, GA, and borneol, while photosystems PSI and II presented associations with stress markers (SOD, CAT) and cell wall degradation (total pectin). Notably, the PSII protein demonstrated a very strong link ($r > 0.9$) with beta-glucans (GBG) and Prx2, reinforcing the interdependence between thylakoid membrane stability and the antioxidant defense system.

The antioxidant defense system exhibited the densest network of strong interactions ($r > 0.7$), where SOD, CAT, and Prx2 varied in close synchrony with E3 ubiquitin ligase, indicating fine-tuned regulation of proteolysis and redox homeostasis. Vitamin C biosynthesis, represented by the GME enzyme, showed a strong correlation ($r > 0.7$) with ATP synthase and GAPDH, suggesting that the fruit's antioxidant potential is dependent on the energy supply derived from primary metabolism. CAT, in particular, presented a very strong correlation with Heat Shock Proteins, linking chemical defense to the physical integrity of the fruit.

Cell wall dynamics were monitored via total and soluble pectin, which showed moderate to strong correlations with most metabolic enzymes and stress proteins. The SAMS enzyme, a key player in ethylene

synthesis, presented very strong associations ($r > 0.9$) with GAPDH and TPI, in addition to strong correlations with aconitate hydratase and GME. This pattern evidences that the hormonal signaling that triggers ripening is metabolically coupled to both carbon supply and ascorbate biosynthesis, as well as pectin restructuring, ensuring that softening and aroma development occur in a synchronized manner.

4. Conclusion

The multi-omics study of *H. dulcis* pseudofruit development reveals a highly coordinated biological system, where maturation is defined by a strategic redirection of carbon and energy flux. This process spans 180 days, with the critical metabolic transition occurring from stage S4 (120–150 DAA) and culminating in effective ripening at S7.

Multivariate analysis (PCA and sPLS-DA) consolidated the existence of three distinct phases: chemical defense (S1–S2), metabolic transition (S3–S6), and sensory maturation (S7). This stratification is governed by a dense network of molecular interactions, with central metabolism (glycolysis and the Krebs cycle) acting as the integrating axis. The strong synchrony observed between glycolytic enzymes (GAPDH, TPI, PGK) and the antioxidant defense system (SOD, CAT, Prx2) demonstrates that the pseudofruit maintains fine-tuned regulation of redox homeostasis and energy supply to sustain secondary metabolite synthesis and cell wall restructuring.

Determining phenological events, such as the reduction in Hue angle (H) and the increase in density, were statistically validated by high VIP scores and Comp 1 loadings, highlighting the central role of the malate dehydrogenase (MDH) enzyme in flavor transition and biomass accumulation. Simultaneously, the evolution of the volatile profile from green notes in early stages to complex esters at maturity evidences a specialization of sensory attributes aimed at attractivity for dispersers.

The robustness of the proteometabolic integration is confirmed by strong Pearson correlations, which revealed the coupling between hormonal signaling (via the SAMS enzyme), polysaccharide degradation, and ascorbate synthesis. Together, these results not only decipher the molecular determinants of programmed senescence in *H. dulcis* but also provide a solid scientific basis for selecting the ideal harvest stage, enabling the strategic technological and nutritional utilization of this pseudofruit to meet the demands of the functional food industry.

CRediT authorship contribution statement

Gilson Gustavo Lucinda Machado: Writing – original draft, Software, Methodology, Investigation, Data curation, Conceptualization. **Elda Eller:** Writing – review & editing, Visualization. **Carlos Henrique Milagres Ribeiro:** Methodology, Investigation. **Carlos Alexandre Rocha da Costa:** Methodology, Investigation. **Sidney Vasconcelos do Nascimento:** Methodology, Investigation. **Sayure Mariana Raad Nahon:** Methodology, Investigation. **Alice de Paula de Sousa Cavalcante:** Methodology, Investigation. **Isa Rebecca Chagas da Costa:** Methodology, Investigation. **Rafael Borges da Silva Valadares:** Methodology, Investigation. **Elisângela Elena Nunes Carvalho:** Methodology, Investigation. **Eduardo Valério de Barros Vilas Boas:** Writing – original draft, Visualization, Validation, Supervision, Project administration, Funding acquisition, Conceptualization.

Funding

This work was supported by the FAPEMIG, Fundação de Amparo à Pesquisa do Estado de Minas Gerais [PPM-00355-17]; Conselho Nacional de Desenvolvimento Científico e Tecnológico [302699/2019–8;404716/2021–0]; and Coordenação de Aperfeiçoamento de Pessoal de Nível Superior [88881.068456/2014–01; 88881.200497/2018–01].

Declaration of competing interest

The authors declare that they have no known competing financial interests or personal relationships that could have appeared to influence the work reported in this paper.

Acknowledgements

The authors would like to thank the Central of Analysis and Chemical Prospecting of the Federal University of Lavras, and the Vale Technological Institute for the support. Finep, To The National Council of Technological and Scientifc Development (CNPq:304413/2016-0; 302699/2019-8), the Minas Gerais Research Support Foundation (FAPEMIG: PPM-00458-15; PPM-00355-17), and the Higher Education Personnel Improvement Coordination (CAPES: 88881.068456/2014-01) for financial support.

Appendix A. Supplementary data

Supplementary data to this article can be found online at https://doi.org/10.1016/j.fochms.2026.100407.

Data availability

Data will be made available on request.

References

Aharoni, A., Jongsma, M. A., Kim, T.-Y., Ri, M.-B., Giri, A. P., Verstappen, F. W. A., … Bouwmeester, H. J. (2006). Metabolic engineering of terpenoid biosynthesis in plants. *Phytochemistry Reviews, 5*(1), 49–58. https://doi.org/10.1007/s11101-005-3747-3

Al-Whaibi, M. H. (2011). Plant heat-shock proteins: A mini review. *Journal of King Saud University – Science, 23*(2), 139–150. https://doi.org/10.1016/j.jksus.2010.06.022

Ambasht, P. K., & Kaystha, A. M. (2002). Plant pyruvate kinase. *Biologia Plantarum, 45*(1), 1–10. https://doi.org/10.1023/A:1015173724712

Association of Official Analytical Chemistry. (2019). *Official methods of analysis* (21st ed.). Gaithersburg: AOAC.

Bae, J., Kim, N., Shin, Y., Kim, S.-Y., & Kim, Y.-M. (2020). Activity of catechins and their applications. *Biomedical Dermatology, 4*(1). https://doi.org/10.1186/s41702-020-0057-8. Article 8.

Barcia, M. T., Pertuzatti, P. B., Jacques, A. C., Godoy, H. T., & Zambiasi, R. (2012). Bioactive compounds, antioxidant activity and percent composition of jambolão fruits (*Syzygium cumini*). *The Natural Products Journal, 12*(2), 129–138.

Barragán-Iglesias, J., Méndez-Lagunas, L. L., & Rodríguez-Ramírez, J. (2018). Ripeness indexes and physicochemical changes of papaya (*Carica papaya* L. cv. Maradol) during ripening on-tree. *Scientia Horticulturae, 236*, 272–278. https://doi.org/10.1016/j.scienta.2017.12.012

Bate, N. J., & Rothstein, S. J. (1998). C6-volatiles derived from the lipoxygenase pathway induce a subset of defense-related genes. *The Plant Journal, 16*, 561–569. https://doi.org/10.1046/j.1365-313x.1998.00324.x

Beckles, D. M. (2012). Factors affecting the postharvest soluble solids and sugar content of tomato (*Solanum lycopersicum* L.) fruit. *Postharvest Biology and Technology, 63*, 129–140. https://doi.org/10.1016/j.postharvbio.2011.05.016

Berretta, M., Bignucolo, A., Francia, R. D., Comello, F., Facchini, G., Ceccarelli, M., … Maurea, N. (2020). Resveratrol in cancer patients: From bench to bedside. *International Journal of Molecular Sciences, 21*, Article 2945. https://doi.org/10.3390/ijms21082945

Bitter, T., & Muir, H. M. (1962). A modified uronic acid carbazole reaction. *Analytical Biochemistry, 4*(4), 330–334.

Bizzio, L. N., Tieman, D., & Muñoz, P. R. (2022). Branched-chain volatiles in fruit: A molecular perspective. *Frontiers in Plant Science, 12*, Article 814138. https://doi.org/10.3389/fpls.2021.814138

Bramley, P. M. (2002). Regulation of carotenoid formation during tomato fruit ripening and development. *Journal of Experimental Botany, 53*(377), 2107–2113. https://doi.org/10.1093/jxb/erf059

Carrari, F., Nunes-Nesi, A., Gibon, Y., Lytovchenko, A., Loureiro, M. E., & Fernie, A. R. (2003). Reduced expression of aconitase results in an enhanced rate of photosynthesis and marked shifts in carbon partitioning in illuminated leaves of wild species tomato. *Plant Physiology, 133*(3), 1322–1335. https://doi.org/10.1104/pp.103.026716

Celi, G. E. A., Gratão, P. L., Lanza, M. G. D. B., & Reis, A. R. D. (2023). Physiological and biochemical roles of ascorbic acid on mitigation of abiotic stresses in plants. *Plant Physiology and Biochemistry, 202*, Article 107970. https://doi.org/10.1016/j.plaphy.2023.107970

Chen, C. H., Wang, C. C., Liu, Z. X., Cai, Z. C., Hua, Y., Mei, Y., … Liu, X. (2020). ITRAQ-based proteomic technique provides insights into salt stress responsive proteins in

Apocyni Veneti Folium (*Apocynum venetum* L.). *Environmental and Experimental Botany, 180*, Article 12. https://doi.org/10.22541/au.158758065.50008650
Choi, H. G., Park, D. Y., & Kang, N. J. (2022). The fruit proteome response to the ripening stages in three tomato genotypes. *Plants, 11*(533), 1–18. https://doi.org/10.3390/plants11040553
Choi, R. Y., Woo, M. J., Ham, J. R., & Lee, M. K. (2017). Anti-steatotic and anti-inflammatory effects of *Hovenia dulcis* Thunb. extracts in chronic alcohol-fed rats. *Biomedicine and Pharmacotherapy, 90*, 393–401. https://doi.org/10.1016/j.biopha.2017.03.077
Cordenunsi-Lysenko, B. R., Nascimento, J. R. O., Castro-Alves, V. C., Purgatto, E., Fabi, J. P., & Peroni-Okita, F. H. G. (2019). The starch is (not) just another brick in the wall: The primary metabolism of sugars during banana ripening. *Frontiers in Plant Science, 10*, Article 391. https://doi.org/10.3389/fpls.2019.00391
Da Costa, C. A. R., do Nascimento, S. V., Valadares, R. B.d. S., da Silva, L. G. M., Machado, G. G. L., Da Costa, I. R. C., … Boas, E. V.d. B. V. (2024). Proteome and metabolome of *Caryocar brasiliense* Camb. fruit and their interaction during development. *Food Research International, 191*, Article 114687. https://doi.org/10.1016/j.foodres.2024.114687
Da Costa, C. A. R., Machado, G. G. L., Rodrigues, L. J., De Barros, H. E. A., Natarelli, C. V. L., & Boas, E. V. B. V. (2023). Phenolic compounds profile and antioxidant activity of purple passion fruit's pulp, peel, and seed at different maturation stages. *Scientia Horticulturae, 321*, Article 112244. https://doi.org/10.1016/j.scienta.2023.112244
Da Costa, C. A. R., Nascimento, S. V., Valadares, R. B.d. S., da Silva, L. G. M., Machado, G. G. L., Cavalcante, A.d. P.d. S., … Boas, E. V.d. B. V. (2025). Proteome and metabolome of *Annona crassiflora* Mart. fruit and their interaction during development. *Scientia Horticulturae, 339*, Article 113809. https://doi.org/10.1016/j.scienta.2024.113809
Da Costa, C. A. R., Silva, L. G. M., Barros, A. G., Machado, G. G. L., Galdino, M. L. S., Amorim, K. A., … Vilas Boas, E. V. B. (2025). Characterization of volatile organic compounds profile and prediction of pharmacokinetic properties by ADMET in purple passion fruit (*Passiflora edulis* Sims) pulp at different maturation stages. *Acta Scientific Nutritional Health, 9*(9), Article 1562. https://doi.org/10.31080/ASNH.2025.09.1562
De Biaggi, M., Donno, D., Mellano, M. G., Gamba, G., Riondato, I., Rakotoniaina, E. N., & Beccaro, G. L. (2020). Emerging species with nutraceutical properties: Bioactive compounds from *Hovenia dulcis* pseudofruits. *Food Chemistry, 310*, 1–10. https://doi.org/10.1016/j.foodchem.2019.125816
De Godoi, R. S., Almerão, M. P., & da Silva, F. R. (2021). In silico evaluation of the antidiabetic activity of natural compounds from *Hovenia dulcis* Thunberg. *Journal of Herbal Medicine, 28*, 1–8. https://doi.org/10.1016/j.hermed.2020.100349
Dische, Z. (1962). General color reactions. In R. L. Whistler, & M. L. Wolfram (Eds.), *Carbohydrate chemistry* (pp. 477–512). New York: Academic Press.
Do Nascimento, S. V., Costa, P. H. de O., Herrera, H., Caldeira, C. F., Gastauer, M., Ramos, S. J., Oliveira, G., & Valadares, R. B. da S. (2022). Proteomic profiling and rhizosphere-associated microbial communities reveal adaptive mechanisms of *Dioclea apurensis* Kunth in eastern Amazon's rehabilitating minelands. *Plants, 11*(5). Doi: https://doi.org/10.3390/plants11050712.
El Hadi, M. A. M., Zhang, F.-J., Wu, F.-F., Zhou, C.-H., & Tao, J. (2013). Advances in fruit aroma volatile research. *Molecules, 18*(7), 8200–8229. https://doi.org/10.3390/molecules18078200
Ferreira, D. F. (2010). *SISVAR - Sistema de análise de variância* (Versão 5.8). Lavras: UFLA.
Feussner, I., & Wasternack, C. (2002). The lipoxygenase pathway. *Annual Review of Plant Biology, 53*(1), 275–297. https://doi.org/10.1146/annurev.arplant.53.100301.135248
Garrido, A., Conde, A., Serôdio, J., De Vos, R. C. H., & Cunha, A. (2023). Fruit photosynthesis: More to know about where, how and why. *Plants, 12*(13), Article 2393. https://doi.org/10.3390/plants12132393
Gill, S. S., Anjum, N. A., Gill, R., Yadav, S., Hasanuzzaman, M., Fujita, M., … Tuteja, N. (2015). Superoxide dismutase – Mentor of abiotic stress tolerance in crop plants. *Environmental Science and Pollution Research, 22*, 10375–10394. https://doi.org/10.1007/s11356-015-4532-5
Han, Y., & Barringer, S. (2016). Formation of volatiles in the lipoxygenase pathway as affected by fruit type and temperature. *Journal of Experimental Food Chemistry, 1*(1), Article 102. https://doi.org/10.4172/2472-0542.1000102
Hasan, M., & Bae, H. (2017). An overview of stress-induced resveratrol synthesis in grapes: Perspectives for resveratrol-enriched grape products. *Molecules, 22*(2), Article 294. https://doi.org/10.3390/molecules22020294
Jiang, L., Kang, R., Feng, L., Yu, Z., & Luo, H. (2020). iTRAQ-based quantitative proteomic analysis of peach fruit (*Prunus persica* L.) at different ripening and postharvest storage stages. *Postharvest Biology and Technology, 164*, Article 111137. https://doi.org/10.1016/j.postharvbio.2020.111137
Kapoor, L., Simkin, A. J., Doss, C. G. P., & Siva, R. (2022). Fruit ripening: Dynamics and integrated analysis of carotenoids and anthocyanins. *BMC Plant Biology, 22*(27), 1–22. https://doi.org/10.1186/s12870-021-03411-w
Kebede, A., & Kebede, M. (2021). In silico analysis of promoter region and regulatory elements of glucan endo–1,3-beta-glucosidase encoding genes in *Solanum tuberosum*: Cultivar DM 1–3 516 R44. *Journal of Genetic Engineering and Biotechnology, 19*(1), Article 145. https://doi.org/10.1186/s43141-021-00240-0
Kim, H., Kim, Y. J., Jeong, H. Y., Kim, J. Y., Choi, E. K., Chae, S. W., & Kwon, O. (2017). A standardized extract of the fruit of *Hovenia dulcis* alleviated alcohol-induced hangover in healthy subjects with heterozygous ALDH2: A randomized, controlled, crossover trial. *Journal of Ethnopharmacology, 209*, 167–174. https://doi.org/10.1016/j.jep.2017.07.028
Kim, S.-H., Lee, J.-W., & Huh, C.-K. (2023). Comparative analysis of nutritional components in various parts of *Hovenia dulcis* Thunbergii. *Korean Journal of Food Preservation, 30*(1), 1–14. https://doi.org/10.11002/kjfp.2023.30.1.1
Kochetov, G. A., & Solovjeva, O. N. (2014). Structure and functioning mechanism of transketolase. *Biochimica et Biophysica Acta, 1844*, 1608–1618. https://doi.org/10.1016/j.bbapap.2014.06.003
Lee, D. H. Y., & Francis, F. J. (1972). Standardization of pigment analyses in cranberries. *HortScience, 7*(1), 83–84.
Li, W., Wang, H., Xu, Q., Zhang, L., Wang, Y., Yu, Y., Guo, X., Zhang, Z., Dong, Y., & Li, Y. (2014). The cytosolic isoform of triosephosphate isomerase, ZmTPI4, is required for kernel development and starch synthesis in maize (*Zea mays* L.). *The Crop Journal, 12*, 401–410. https://doi.org/10.1016/j.cj.2024.02.001
Li, Y., Lu, L., Zhang, X., Mu, Q., Tian, J., Yan, J., Guo, L., Wang, Y., Song, L., & Yu, X. (2023). Differences in total phenolics, antioxidant activity and metabolic characteristics in peach fruits at different stages of ripening. *LWT – Food Science and Technology, 178*, Article 114586. https://doi.org/10.1016/j.lwt.2023.114586
Liu, T., Arsenault, J., Vierling, E., & Kim, M. (2021). Mitochondrial ATP synthase subunit d, a component of the peripheral stalk, is essential for growth and heat stress tolerance in *Arabidopsis thaliana*. *The Plant Journal, 107*, 713–726. https://doi.org/10.1111/tpj.15317
Luo, Y., Ge, C., Yang, M., Long, Y., Li, M., Zhang, Y., Chen, Q., Sun, B., Wang, Y., Wang, X., & Tang, H. (2020). Cytosolic/plastid glyceraldehyde-3-phosphate dehydrogenase is a negative regulator of strawberry fruit ripening. *Genes, 11*(580), 1–10. https://doi.org/https://doi.org/10.3390/genes11050580.
Lv, M., Zhang, L., Wang, Y., Ma, L., Yang, Y., Zhou, X., Wang, L., Yu, X., & Li, S. (2024). Floral volatile benzenoids/phenylpropanoids: biosynthetic pathway, regulation and ecological value. *Horticulture Research, 11*, Article uhae220. https://doi.org/10.1093/hr/uhae220
Machado, G. G. L., Arruda, K. A. C., Luna, C. E., & Gonçalves, G. A. S. (2022). Pseudofrutos de *Hovenia dulcis* Thunb. de Minas Gerais. *ForScience, 10*(2), Article e01072. https://doi.org/10.29069/forscience.2022v10n2.e1072
Machado, G. G. L., Da Costa, C. A. R., Do Nascimento, S. V., Nahon, S. M. R., Cavalcante, A. P. S., da Costa, I. R. C., … Boas, E. V. B. V. (2025). Metabolomics and proteomics of Campomanesia pubescens fruits throughout developmental stages. *Food Chemistry, 485*, Article 144479. https://doi.org/10.1016/j.foodchem.2025.144479
Machado, G. G. L., de Barros, H. E. A., Natarelli, C. V. L., Araújo, A. B. S., Ribeiro, C. H. M., & Boas, E. V. B. V. (2024). Gabiroba (*Campomanesia pubescens*): Physicochemical and physiological characteristics of fruit during development. *Revista Brasileira de Ciências Agrárias, 19*(2), Article e3583. https://doi.org/10.5039/agraria.v19i2a3583
Machado, G. G. L., & Gonçalves, G. A. S. (2021). *Hovenia dulcis* - Development and evaluation of jelly and dehydrated fruit. *Carpathian Journal of Food Science and Technology, 13*(1), 90–100. https://doi.org/10.34302/crpjfst/2021.13.1.8
Maieves, H. A., Bosmuler Züge, L. C., Scheer, A. D. P., Ribani, R. H., Morales, P., & Sánchez-Mata, M. C. (2017). Physical properties and rheological behavior of pseudofruits of *Hovenia dulcis* Thunb. in different maturity stages. *Journal of Texture Studies, 48*(1), 31–38. https://doi.org/10.1111/jtxs.12199
Maieves, H. A., Ribani, R. H., Morales, P., & Sánchez-Mata, M. C. (2015). Evolution of the nutritional composition of *Hovenia dulcis* Thunb. pseudofruit during the maturation process. *Fruits, 70*(3), 181–187. https://doi.org/10.1051/fruits/2015011.
Mao, X., Yu, C., Li, L., Wang, M., Yang, L., Zhang, Y., … Jing, R. (2022). How many faces does the plant U-box E3 ligase have? *International Journal of Molecular Sciences, 23*(4), 2285. https://doi.org/10.3390/ijms23042285
Masia, A. (1998). Superoxide dismutase and catalase activities in apple fruit during ripening and post-harvest, with special reference to ethylene. *Physiologia Plantarum, 104*, 668–672. https://doi.org/10.1034/j.1399-3054.1998.1040421.x
McCreaddy, R. M., & McComb, E. A. (1952). Extraction and determination of total pectic materials in fruits. *Analytical Chemistry, 24*(12), 1986–1988.
Mellidou, I., Keulemans, J., Kanellis, A. K., & Davey, M. W. (2012). Regulation of fruit ascorbic acid concentrations during ripening in high and low vitamin C tomato cultivars. *BMC Plant Biology, 12*(239), 1–19. https://doi.org/10.1186/1471-2229-12-239
Meng, X., Tang, G.-Y., Zhao, C.-N., Liu, Q., Xu, X.-Y., & Cao, S.-Y. (2020). Hepatoprotective effects of *Hovenia dulcis* seeds against alcoholic liver injury and related mechanisms investigated via network pharmacology. *World Journal of Gastroenterology, 26*(24), 3432–3446. https://doi.org/10.3748/wjg.v26.i24.3432
Mhamdi, A., Queval, G., Chaouch, S., Vanderauwera, S., Breusegem, F. V., & Noctor, G. (2010). Catalase function in plants: A focus on *Arabidopsis* mutants as stress-mimic models. *Journal of Experimental Botany, 61*(15), 4197–4220. https://doi.org/10.1093/jxb/erq282
Morales, P., Maieves, H. A., Dias, M. I., Calhella, R. C., Sánchez-Mata, M. C., Santos-Buelga, C., … Ferreira, I. C. F. R. (2017). Hovenia dulcis Thunb. pseudofruits as functional foods: Phytochemicals and bioactive properties in different maturity stages. *Journal of Functional Foods, 29*, 37–45. https://doi.org/10.1016/j.jff.2016.12.003
Oh, K. N., Kim, Y., Choi, E. J., Lee, H., Hong, J. A., Kim, M., … Choi, C. Y. (2020). Laxative activity of the hot-water extract mixture of *Hovenia dulcis* Thunb. and *Phyllostachys pubescens* Mazel in chronic constipation model SD rats. *Journal of Microbiology and Biotechnology, 30*(5), 649–661. https://doi.org/10.4014/jmb.1911.11051
Paradiso, V. M., Castellino, M., Renna, M., Gattullo, C. E., Calasso, M., Terzano, R., … Santamaria, P. (2018). Nutritional characterization and shelf-life of packaged microgreens. *Food & Function, 9*(11), 5629–5640. https://doi.org/10.1039/C8FO01182F

Peng, H., Deng, Z., Chen, X., Sun, Y., Zhang, B., & Li, H. (2018). Major chemical constituents and antioxidant activities of different extracts from the peduncles of *Hovenia acerba* Lindl. *International Journal of Food Properties, 21*(1), 2135–2155. https://doi.org/10.1080/10942912.2018.1497059

Pinto, J. T., Alvarenga, L. F., de Oliveira, D. P., de Oliveira, T. T., Schwan, R. F., Dias, D. R., & de Queiroz, J. H. (2017). Elaboration and characterization of Japanese Raisin Tree (*Hovenia dulcis* Thumb.) pseudofruits fermented alcoholic beverage. *Food Science and Technology, 37*(1), 101–108. https://doi.org/10.1590/1678-457x.25616

Qian, X., Liu, Y., Zhang, G., Yan, A., Wong, W.-L., Wang, X., Pan, Q., Xu, H., Sun, L., & Zhu, B. (2019). Alcohol acyltransferase gene and ester precursors differentiate composition of volatile esters in three interspecific hybrids of *Vitis labrusca* × *V. vinifera* during berry development period. *Food Chemistry, 295*, 234–246. https://doi.org/10.1016/j.foodchem.2019.05.104

Qiu, P., Dong, Y., Zhu, T., Luo, Y. Y., Kang, X. J., Pang, M. X., … Ge, W. H. (2019). Semen hoveniae extract ameliorates alcohol-induced chronic liver damage in rats via modulation of the abnormalities of gut-liver axis. *Phytomedicine, 52*, 40–50. https://doi.org/10.1016/j.phymed.2018.09.209

Ramos, O. L., & Malcata, F. X. (2010). Food-grade enzymes. In M. Moo-Young (Ed.), *Comprehensive Biotechnology* (2nd ed., pp. 555–569). Elsevier. https://doi.org/10.1016/B978-0-08-088504-9.00213-0.

Rane, J., Babar, R., Kumar, M., Kumar, P. S., Singh, Y., Nangare, D. D., … Minhas, P. S. (2021). Desiccation tolerance of Photosystem II in dryland fruit crops. *Scientia Horticulturae, 288*, Article 110295. https://doi.org/10.1016/j.scienta.2021.110295

Rashidi, R., Rezaee, R., Shakeri, A., Hayes, A. W., & Karimi, G. (2022). A review of the protective effects of chlorogenic acid against different chemicals. *Journal of Food Biochemistry, 46*(9), Article e14254. https://doi.org/10.1111/jfbc.14254

Rodriguez-Amaya, D. B. (2001). *A guide to carotenoid analysis in foods*. Washington: International Life Sciences Institute Press.

Rosenkranz, M., Chen, Y., Zhu, P., & Vlot, A. C. (2021). Volatile terpenes – Mediators of plant-to-plant communication. *The Plant Journal, 108*(3), 617–631. https://doi.org/10.1111/tpj.15453

Saltveit, M. E. (2019). Respiratory metabolism. In E. M. Yahia, & A. Carrillo-López (Eds.), *Postharvest physiology and biochemistry of fruits and vegetables* (pp. 73–91). Elsevier. https://doi.org/10.1016/B978-0-12-813278-4.00004-X.

Schaefer, S. V., do Amaral, A. M. P., Cherobin, A. K., Monteiro, L. K., Morandin, G. C., Fischer, C., … Sehn, G. A. R. (2022). Japanese grape (*Hovenia dulcis*) powder as an antioxidant agent in Bologna sausages. *Journal of the Science of Food and Agriculture, 102*(14), 6255–6262. https://doi.org/10.1002/jsfa.11974

Schwab, W., Davidovich-Rikanati, R., & Lewinsohn, E. (2008). Biosynthesis of plant-derived flavor compounds. *The Plant Journal, 54*(4), 712–732. https://doi.org/10.1111/j.1365-313X.2008.03446.x

Sehn, G. A. R., Schaefer, S. V., Schmiele, M., da Silva, B. P., Barcia, M. T., & Rodrigues, R. S. (2021). Characterization of pseudo-fruits of *Hovenia dulcis* T. at different maturation stages and drying methods. *Acta Scientiarum, 43*, Article e50571. https://doi.org/10.4025/actascitechnol.v43i1.50571

Sferrazza, G., Brusotti, G., Zonfrillo, M., Temporini, C., Tengattini, S., Bononi, M., Tateo, F., Calleri, E., & Pierimarchi, P. (2021). Hovenia dulcis Thunberg: Phytochemistry, pharmacology, toxicology and regulatory framework for its use in the European Union. *Molecules, 26*(4), Article 903. https://doi.org/10.3390/molecules26040903

Singh, A., Gupta, R., & Pandey, R. (2017). Exogenous application of rutin and gallic acid regulate antioxidants and alleviate reactive oxygen generation in *Oryza sativa* L. *Physiology and Molecular Biology of Plants, 23*(2), 301–309. https://doi.org/10.1007/s12298-017-0430-2

Smirnoff, N., Conklin, P. L., & Loewus, F. A. (2001). Biosynthesis of ascorbic acid in plants: A renaissance. *Annual Review of Plant Physiology and Plant Molecular Biology, 52*, 437–467. https://doi.org/10.1146/annurev.arplant.52.1.437

Song, G., Kim, H. L., Jung, Y., Park, J., Lee, J. H., Ahn, K. S., … Um, J. Y. (2020). Fruit of *Hovenia dulcis* Thunb. induces nonshivering thermogenesis through mitochondrial biogenesis and activation by SIRT1 in high-fat diet-fed obese mice and primary cultured brown adipocytes. *Journal of Agricultural and Food Chemistry, 68*(25), 6715–6725. https://doi.org/10.1021/acs.jafc.0c01117

Srinivasulu, C., Ramgopal, M., Ramanjaneyulu, G., Anuradha, C. M., & Suresh Kumar, C. (2018). Syringic acid (SA) – A review of its occurrence, biosynthesis, pharmacological and industrial importance. *Biomedicine & Pharmacotherapy, 108*, 547–557. https://doi.org/10.1016/j.biopha.2018.09.069

Stroheker, R., & Henning, H. M. (1967). *Análisis de vitaminas: Métodos comprobados*. Madrid: Paz Montalvo.

Thi Ngo, Q. M., Ha, M. T., Vu, N. K., Kim, J. A., Woo, M. H., & Min, B. S. (2021). Constituents from the pseudofruits of *Hovenia dulcis* and their chemotaxonomic significance. *Biochemical Systematics and Ecology, 94*, Article 104221. https://doi.org/10.1016/j.bse.2020.104221

Tutar, L., & Tutar, Y. (2011). Heat shock proteins: An overview. *Current Pharmaceutical Biotechnology, 11*(2), 216–222. https://doi.org/10.2174/138920110790909632

Vanholme, R., De Meester, B., Ralph, J., & Boerjan, W. (2019). Lignin biosynthesis and its integration into metabolism. *Current Opinion in Biotechnology, 56*, 230–239. https://doi.org/10.1016/j.copbio.2019.02.018

Vogt, T. (2010). Phenylpropanoid biosynthesis. *Molecular Plant, 3*(1), 2–20. https://doi.org/10.1093/mp/ssp106

Wang, H., Qian, Z., Ma, S., Zhou, Y., Patrick, J. W., Duan, X., … Qu, H. (2013). Energy status of ripening and postharvest senescent fruit of litchi (*Litchi chinensis* Sonn). *BMC Plant Biology, 13*(55), 1–16. https://doi.org/10.1186/1471-2229-13-55

Wang, H., Zheng, X., Wu, Y., Zhan, W., Guo, Y., Chen, M., Bai, T., Jiao, J., Song, C., & Song, S. (2023). Transcriptome analysis identifies genes associated with chlorogenic acid biosynthesis during apple fruit development. *Horticulturae, 9*(2), 217–230. https://doi.org/10.3390/horticulturae9020217

Wang, M., Liu, Y., Qiang, M., & Wang, J. (2017). Structural elucidation of a pectin-type polysaccharide from *Hovenia dulcis* peduncles and its proliferative activity on RAW264.7 cells. *International Journal of Biological Macromolecules, 104*, 1246–1253. https://doi.org/10.1016/j.ijbiomac.2017.07.004

Xu, F., Gao, M., Li, H., Han, X., Zhang, X., Li, Y., … Liu, B. (2020). Three new bisflavonols from the seeds of *Hovenia dulcis* Thunb. and their anti-RSV activities. *Fitoterapia, 143*, Article 104587. https://doi.org/10.1016/j.fitote.2020.104587

Yang, B., Wu, Q., Luo, Y., Yang, Q., Chen, G., Wei, X., & Kan, J. (2019). Japanese grape (*Hovenia dulcis*) polysaccharides: New insight into extraction, characterization, rheological properties, and bioactivities. *International Journal of Biological Macromolecules, 134*, 631–644. https://doi.org/10.1016/j.ijbiomac.2019.05.079

Yao, H., Gu, Y., Zhu, D., Tang, D., Chen, W., Chen, Y., Zhang, J., & Tan, L. (2025). Biosynthesis and application of catechins and their derivatives in *Camellia sinensis*. *Food Science & Nutrition, 13*(12), Article e71277. https://doi.org/10.1002/fsn3.71277

Yao, Y. X., Li, M., Zhai, H., You, C. X., & Hao, Y. J. (2011). Isolation and characterization of an apple cytosolic malate dehydrogenase gene reveal its function in malate synthesis. *Journal of Plant Physiology, 168*, 474–480. https://doi.org/10.1016/j.jplph.2010.08.008

Yazar, M., Sevindik, M., Uysal, I., & Akpinar, K. (2025). Effects of caffeic acid on human health: Pharmacological and therapeutic effects, biological activity and toxicity. *Pharmaceutical Chemistry Journal, 59*(1), 49–55. https://doi.org/10.1007/s11094-025-03363-7

Yu, Y., Zhang, Z., & Chang, C. (2022). Chlorogenic acid intake guidance: Sources, health benefits, and safety. *Asia Pacific Journal of Clinical Nutrition, 31*(4), 602–610. https://doi.org/10.6133/apjcn.202212_31(4).0003

Yun, Z., Li, W., Pan, Z., Xu, J., Cheng, Y., & Deng, X. (2010). Comparative proteomics analysis of differentially accumulated proteins in juice sacs of ponkan (*Citrus reticulata*) fruit during postharvest cold storage. *Postharvest Biology and Technology, 56*, 189–201. https://doi.org/10.1016/j.postharvbio.2010.01.002

Zanandrea, I., Alves, J. D., Deuner, S., de Goulart, P. F. P., de Henrique, P. C., & Silveira, N. M. T. (2009). Tolerance of *Sesbania virgata* plants to flooding. *Australian Journal of Botany, 57*(8), 661–669.

Zhang, L., Ma, B., Wang, C., Chen, X., Ruan, Y. L., Yuan, Y., … Li, M. (2022). MdWRKY126 modulates malate accumulation in apple fruit by regulating cytosolic malate dehydrogenase (MdMDH5). *Plant Physiology, 188*(4), 2059–2072. https://doi.org/10.1093/plphys/kiac023

Zhou, Z.-W., Wu, Q.-Y., Ni, Z.-X., Hu, Q.-C., Yang, Y., Zheng, Y.-C., Bi, W.-J., Deng, H.-L., Liu, Z.-Z., Ye, N.-X., Lai, Z.-X., & Sun, Y. (2021). Metabolic flow of C6 volatile compounds from LOX-HPL pathway based on airflow during the post-harvest process of oolong tea. *Frontiers in Plant Science, 12*, Article 738445. https://doi.org/10.3389/fpls.2021.738445

Zhu, J., Deng, Y., Zhang, X., Zhou, X., Sang, Y., & Yang, B. (2025). Quercetin-*Hovenia dulcis* polysaccharide complexes inhibit α-glucosidase and mitigate hyperglycemia. *International Journal of Biological Macromolecules, 327*, Article 147390. https://doi.org/10.1016/j.ijbiomac.2025.147390